UNIVERSITI MALAYSIA PAHANG

BORANG PENGESAHAN STATUS TESIS♦

JUDUL: **AN EFFECTIVE DESING OF SUN TRACKING SYSTEM TO INCREASE THE PERFORMANCE OF SOLAR CELLS**

SESI PENGAJIAN: **2010/2011**

Saya **LAI WENG HONG (870406-14-5605)**
(HURUF BESAR)

mengaku membenarkan tesis (Sarjana Muda/~~Sarjana~~ /~~Doktor Falsafah~~)* ini disimpan di Perpustakaan dengan syarat-syarat kegunaan seperti berikut:

1. Tesis adalah hakmilik Universiti Malaysia Pahang (UMP).
2. Perpustakaan dibenarkan membuat salinan untuk tujuan pengajian sahaja.
3. Perpustakaan dibenarkan membuat salinan tesis ini sebagai bahan pertukaran antara institusi pengajian tinggi.
4. **Sila tandakan (√)

[ ]	**SULIT**	(Mengandungi maklumat yang berdarjah keselamatan atau kepentingan Malaysia seperti yang termaktub di dalam AKTA RAHSIA RASMI 1972)
[ ]	**TERHAD**	(Mengandungi maklumat TERHAD yang telah ditentukan oleh organisasi/badan di mana penyelidikan dijalankan)
[√]	**TIDAK TERHAD**	

Disahkan oleh:

(TANDATANGAN PENULIS) (TANDATANGAN PENYELIA)

Alamat Tetap:

NO.56, JLN. 1/6,
46000 PETALING JAYA,
SELANGOR.

DR. AHMED MOHAMED AHMED HAIDAR
(Nama Penyelia)

Tarikh: **29 NOVEMBER 2010** Tarikh: : **29 NOVEMBER 2010**

CATATAN:
* Potong yang tidak berkenaan.
** **Jika tesis ini SULIT atau TERHAD, sila lampirkan** surat daripada pihak berkuasa/organisasi berkenaan dengan menyatakan sekali tempoh tesis ini perlu dikelaskan sebagai atau TERHAD.
♦ Tesis dimaksudkan sebagai tesis bagi Ijazah doktor Falsafah dan Sarjana secara Penyelidikan, atau disertasi bagi pengajian secara kerja kursus dan penyelidikan, atau Laporan Projek Sarjana Muda (PSM).

"I hereby declare that I have read this thesis and in my opinion this thesis is sufficient in terms of scope and quality for the award of the degree of Bachelor of Electrical Engineering (Power system)

Signature	: ....
Name of Supervisor	: Dr. Ahmed Mohamed Ahmed Haidar
Date	: 29 November 2010

AN EFFECTIVE DESIGN OF SUN TRAKING SYSTEM TO INCREASE THE PERFORMANCE OF SOLAR CELLS

LAI WENG HONG

This thesis is submitted
As partial fulfillment of the requirements for the award of the degree of
Bachelor of Electrical Engineering (Power System)

Faculty of Electrical & Electronics Engineering
University Malaysia Pahang

NOVEMBER, 2010

Signature : ______________________________

Author : LAI WENG HONG

Date : 29 NOVEMBER 2010

DEDICATION

Specially dedicated to

My beloved family, and those who have guided and inspired me

Through my journey of learning

ACKNOWLEDGEMENT

Throughout the development of this project, I have gained chances to gain new knowledge and skills. First and foremost, I wish to express my sincere appreciation to my supervisor, Dr. Ahmed Mohamed Ahmed Haidar for the encouragement, guidance, suggestions, critics and friendship throughout finishing this project.

Secondly, I wish to thank lecturers, staffs and technicians, for their cooperation and efforts which always nurture us with precious advices and also contribute in finishing my project.

Special thanks to University Malaysia Pahang for supporting and providing equipment and information sources that assisted my studies and projects.

Most importantly, I am grateful to my parents for their support, encouragement, understanding, sacrifice and love.

Lastly I want to thanks all my friends, who directly and indirectly helped me in this project, especially to those who dedicated their knowledge and time for the success of this project.

ABSTRACT

Solar energy is the sun’s rays (solar radiation) that reach the earth. In tropical countries, solar energy potential in wide range of application for remote urban areas is growing rapidly. The major disadvantage of solar energy is the amount of sunlight that arrives at the earth’s surface is not constant. It depends on location, time of day, time of year and weather conditions. In addition, the sun doesn’t deliver that much energy to any exact place at one time, a large surface area is required to collect the energy at a useful rate. Most of the current technology applies only static solar cells that cannot response to the actual instant position of the sun for maximum sun shine. The objective of this work is to design an effective Sun Tracking System that would increase the performance of Solar Cells. In this research, the compartments considered for the proposed system are Solar Cells, Moving Mechanism and Stepper Motor that will be controlled based on the detector of the sun shine using web-camera. As soon as the sun can be tracked, the voltage, current and power received will always be at the maximum efficiency. This research could provide significant improvement in alternative energy as seen from the results which are given in this thesis.

ABSTRAK

Tenaga solar merupakan sinaran matahari (radiasi solar) yang sampai ke bumi. Di negara tropika, applikasi yang meluas bagi potensi tenaga solar untuk kawasan luar bandar tumbuh dengan mendadak. Masalah utama tenaga solar adalah jumlah sinaran matahari yang sampai ke muka bumi tidak malar. Ia bergantung kepada lokasi, masa, musim dan kondisi cuaca. Tambahan, matahari tidak menyampaikan begitu banyak tenaga ke suatu tempat dalam masa tertentu, luas permukaan yang besar diperlukan untuk mengumpul tenaga pada tahap yang berguna. Kebanyakan teknologi semasa hanya mengaplikasikan sel-sel solar static dimana ia tidak dapat bertindakbalas kepada posisi segera matahari yang betul untuk sinaran matahari yang maxima. Objektif projek ini adalah untuk merekakan satu system menjejak matahari yang dapat menambahbaik persembahan sel-sel solar. Dalam kajian ini, bahagian-bahagian yang akan dikaji untuk system yang dicadangkan ialah sel-sel solar, mekanisma bergerak dan juga Stepper Motor yang akan dikawal berdasarkan pengesan sinaran matahari melalui web-kamera. Secepat sahaja matahari dapat dijejak, voltan, arus dan tenaga yang diterima akan menjadikan keberkesanannya sentiasa berada pada tahap maxima. Pengkajian ini dipercayai dapat memberi kemajuan dalam keberkesanan tenaga alternatif seiring dengan keputusan yang didapati dalam tesis ini.

TABLE OF CONTENTS

LIST OF TABLES

LIST OF FIGURES

LIST OF ABBREVIATIONS

AC	Alternating Current
CPC	Compound Parabolic Concentrator
DC	Direct Current
MEMS	Micro-ElectroMechanical System
MOSFET	Metal Oxide Silicon Field Effect Transistor
MPPT	Maximum Power Point Tracker
PIC	Programmable Intelligent Controller
P-N	Positive-Negative
PV	Photovoltaic
PWM	Pulse Width Modulation
ROI	Region of Interest
STS	Solar Tracking System
USB	Universal Serial Bus
V_{pv}	Photovoltaic voltage

CHAPTER 1

INTRODUCTION

1.1 OVERVIEW

In these modern days that consumes a lot of energy, e.g. fuel-oil, gas, coal, that will deplete in its source one day, much focus have been given on the topic of renewable energy. Renewable energies are energy that can be renewed or have no worries of depleting as described by Riza Muhida *et al. (2009)*. For instance, wind, thermal, bio-mass and solar energy are some of the examples for renewable energy. Power station that applied renewable energy as its power source is increasing in number in the recent years. However the current technologies in this field are not competitive enough, when compared to the conventional energy sources such as petroleum fuel, hydroelectric and etc. Solar energy is one of the main renewable energy sources that are widely used in power generating application. It is one of the renewable energy with high availability and at the same time it does not creates much pollution as the conventional power sources. Despite having high availability, the efficiency of the solar cells to convert solar energy into electrical energy is not efficient enough. There are many theories indicated that how the power output efficiency of the solar cells can be improved. Researchers had been conducting many studies on improving the efficiency of the solar cells and there are still spaces for improving the performance of the solar cells.

For a photovoltaic (PV) system, the solar panel is the most important and basic component for the process of energy transformation in solar power system as described by K. K. Tse *et al*. (2004). From the research they conducted, K. K. Tse *et al.* (2004) stated that the energy conversion efficiency of the PV system depends on the external factors. These factors included the insolation (a measure of solar radiation energy received on a given surface area in a given time) level for the specific area, the temperature of the surrounding and also the specification of the load. K. K. Tse *et al.* (2004) also stated that there are a number of different kinds of method were applied to further improve the performance of the solar tracking ability of the system. According to Rong-Jong Wai *et al.* (2008), the major challenges for the engineers and scientists are to obtain a clean, efficient and environmentally-friendly energy sources. Out of so many renewable energy, the researchers discovered that the photovoltaic generation system to be of greatest potential to resolve for energy problem and also environmental problem. Rong-Jong Wai *et al.* (2008) have also pointed out that utilizing the solar power generation system can effectively reduce the effects of environmental concerns such as the air pollution, ozone depletion and radioactive substance emissions.

As described by Roger Gules *et al.* (2008), the exploration of renewable sources such as photovoltaic technology was led by the growing energy demand along with the increasing awareness upon the environment hazards by utilizing the fossil fuels. Roger Gules *et al.* (2008) explained that the main obstacles that prevent the usage of photovoltaic energy source from being utilized in a large scale are because of two factors. One of the factors is the high installation price which is not cost effective. This factor played a main role in preventing more of the public to utilize solar energy generation system. The second factor that obstructed the public from using photovoltaic energy source on a large scale is of its low conversion efficiency. Due to its low conversion efficiency, the utilization so solar energy as the source for generating power is still not as common and popular as the conventional fossil fuels is. There are still spaces available to further enhance the capability of the solar cells to produce electrical energy. Such works and studies have been attempted by researchers in the researching field for exploitation of clean energy resources. Having clean energy resources such as photovoltaic energy resources would help much in reducing the environment pollution problem.

In the research of having a clean and energy-saving system, researchers have found out that solar cell power supply could be used as a reliable power source. Eduardo Roman *et al.* (2006) described that renewable energy resources are technological option for sustainable energy supply and one of the representatives is the photovoltaic energy. Due to technological progress and continuous cost reduction, the solar energy is becoming more common and important towards power generation contribution. Eduardo Roman *et al.* (2006) agreed that the most important element in the photovoltaic generation system is the solar cells. The researchers found out that there are some causes such as shadows, dust, low radiation losses and etc. that are responsible for the low efficiency if power output for the solar power generating system. Eduardo Roman *et al.* (2006) also mentioned that there would be more losses which signified lower efficiency of the solar cells, in case for those installations which are more complex. Such complexity will at the same time brought additional losses to the solar cells. A solar power generating system would pose greater problem when they are complex in number and also configuration.

There are quite a number of factors that would affect the power output efficiency of the solar cells. Work of Jose M. Quero *et al.* (2007) described that the performance of the solar energy power system strongly depends on the ability of the solar power receiver to track the sun. Some systems applied the conventional devices that transform the sun radiation directly into electricity. For example, the conventional photovoltaic cells are capable of transforming the solar radiation into electricity directly. Jose M.

Quero *et al.* (2007) pointed out that the surfaces of the photovoltaic cells must be perpendicular to the sun radiation to achieve maximum performance. They suggested that the direct tracking control for the solar power system should be implemented. Kimiyoshi Kobayashi *et al.* (2006) pointed out that when the solar array is used as the input power source, the light intensity that falls onto the solar cells and the environmental temperature surrounding the solar power generating system would affect the power output efficiency of the solar cells to a certain extent. To achieve a better power output efficiency, the solar cells need to be directed towards the direction of the sun. Having the solar cells directed towards the sun would increase the light intensity that falls onto the solar cells. Thus implementing a solar tracking system for the solar power generating unit would be a good resolve in enhancing the performance of the solar cells.

1.2 RESEARCH OBJECTIVES

This study attempts to achieve the following objectives:

i. To design an effective sun tracking system based on the detector of the sun shine using web-camera.

ii. To analyze and simulate the tracking system using MATLAB interface with the hardware.

iii. To compare the simulation result with the hardware.

1.3 SCOPE OF PROJECT

This project is focused on designing and developing a Solar Tracking System by using web-camera as its sensor. Therefore, the project scopes are as follow:

i. Using MATLAB software to control the movement of the solar tracking system.

ii. Interfacing between the controller and solar tracking system to improve the focus towards sunshine.

1.4 PROBLEM STATEMENT

This study aims to conduct the following research:

i. The sun is moving from east to west trough out the daytime, so the solar irradiation onto the solar cells is varied due to the rotation cycle of the earth. This variation of solar power output decreases the efficiency of the system. Not having a high solar irradiation onto the solar cells would not produce maximum power that the solar cells' capable of.

ii. A static solar power system that does not response instantly to the actual position of the sun does not yield maximum power output from the solar cells. When the earth circulates around the sun, the static solar power system cannot achieve maximum power output as the solar irradiation onto the static solar cells will drop gradually.

1.5 OUTLINE OF THESIS

This thesis consists of five chapters. Chapter one provides introduction on the project. In chapter two, the works done before by the other researchers are reviewed. Chapter three discussed about the methods used in developing the project and also the hardware used. The main focus in chapter four is on the result obtained from the project and discussion of the results. Chapter five concludes the findings and future recommendations for the system.

CHAPTER 2

LITERATURE REVIEW

2.1 Maximum Power Point Tracking

K. K. Tse *et al.* (2004) had used the maximum power point tracker (MPPT) which is also a dc to dc converter, in order to track the maximum power point for the power output from the photovoltaic system. They applied the switching-frequency modulation scheme which injected a small-signal sinusoidal perturbation into the switching frequency of the converter and comparing between the ac component and the average value of the panel terminal voltage. The researchers conducted experiments to study the tracking capability of different dc to dc converter using the switching-frequency modulation scheme. The researchers utilize the solar panel Siemens SM-10 with rated output power of 10 W for the experiment purpose and kept the surface temperature of the panel at about 40 degree celcius throughout the experiment. The illumination of the sun is represented with a 900 W Tungsten halogen lamp, controlled by a programmable dc supply source, PCR 2000L. They conducted a number of different experiments using this method and found out that, the maximum power point tracking with switching-frequency modulation scheme can globally locate the maximum power point for the solar cells under a wide range of insolation level. The capability of locating maximum power point can improve the performance of solar cells up to a certain extent as described by Vikrant. A. Chaudhari (2005). The representation of the work by K. K. Tse *et al.* (2004) was shown in Figure 2.1. The output of the solar panel was sent to the tracking circuit to obtain the maximum power point.

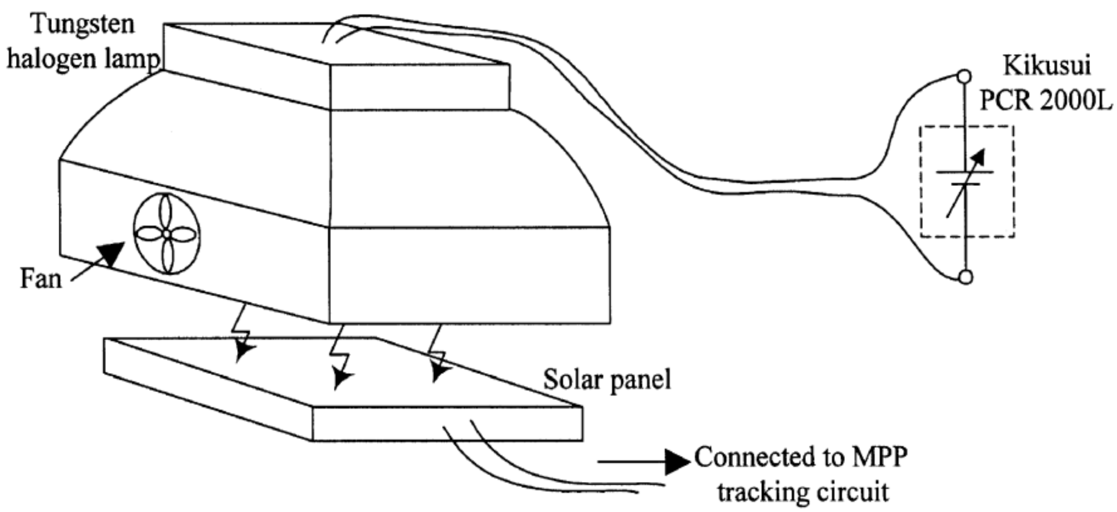

Figure 2.1: Experiment with switching-frequency modulation scheme.

Roger Gules *et al.* (2008) used parallel connection of the maximum power point tracking (MPPT) for the solar power generation system to reduce the power converter losses in the overall power output efficiency of the system. The system designed in this parallel connection of the MPPT circuit as shown in Figure 2.2, possesses the advantage of having only a part of the power generated processed by the dc/dc converter. This means that the load current value is equal to the maximum power point current value for the solar module during the time dc/dc converter does not process power. The system that they designed enables reduction on cost for the electronic components used. Utilization of parallel connection for the solar photovoltaic system with MPPT would enables easier detection of the MPP under imperfect operating condition, such as shading on the PV modules or defection of solar cells. The operation of the MPPT system is aided by the control algorithm designed by the researchers.

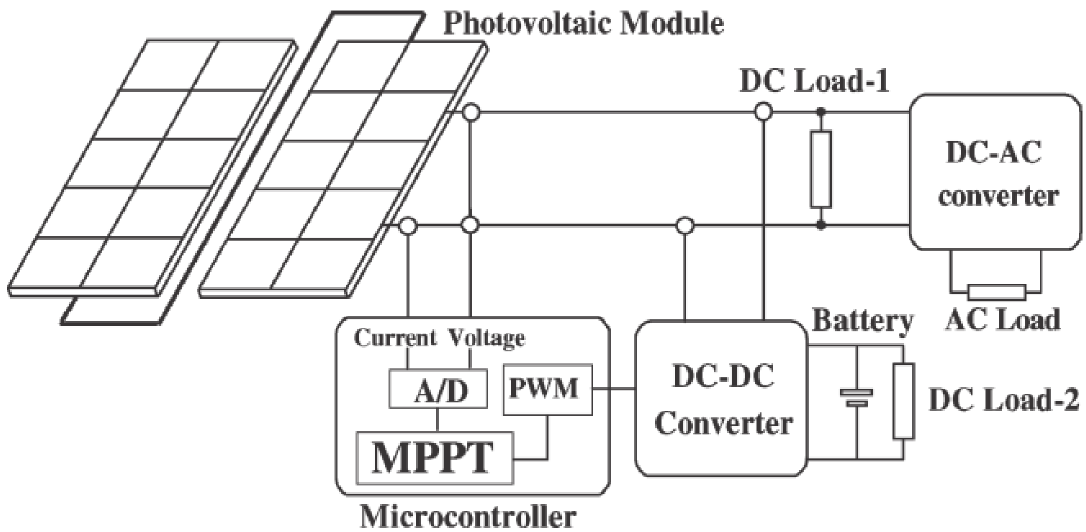

Figure 2.2: Parallel connection of the MPPT in Solar Generation System.

J.M. Enrique *et al.* (2005) concluded that there are limitations in the performance of the system depending on the maximum power point tracking converter used. They studied the buck-boost DC/DC converter which allows the follow-up of the PV module maximum power point independent of the condition of the temperature, irradiance and connected load. They had proven that having a buck-boost DC/DC converter connected to the photovoltaic system can effectively improve the performance of the whole system. The converter used will forces the PV module to operate at the maximum power point, which will overcome the disadvantages due to the high initial installation costs and low energy conversion efficiency of the PV module. Jen-Cheng Wang *et al.* (2010) described that the MPPT circuits can act as the interfaces between the PV systems and the loads.

They said that due to the complexity of mathematical operations involved in the tracking method of maximum power point, micro-controllers are needed to provide control for tracking the maximum power point. They also said that changing the different parameters for the system would affect the operation of the MPPT and thus affecting the efficiency of the PV modules.

Kimiyoshi Kobayashi *et al.* (2006) pointed out that the common method used to track the maximum power point with apparatus such as microcomputer and digital signal processing posted a few problems. The problems meant were the MPPT circuit designed has complex configuration. Other than being expensive, the speed for controlling is low and not efficient. Due to such concerns, they proposed utilization of the p-n junction diodes for generating the reference voltage for the operating point of solar array. P-N junction diodes are inexpensive and affordable. In their work, they discovered that the power output of the solar array is influenced by the light intensity and temperature surrounding the system.

2.2 High Step-up Converter

Work of Rong-Jong Wai *et al.* (2008) stated that, in order to increase the conversion efficiency of the solar cells, the high step-up converter was used to allow the parallel operation of the photovoltaic arrays. The researchers utilize this design to decouple and simplify the control design of the pulse width modulation (PWM) inverter. The V_{pv} (Photovoltaic voltage) is not constant due to the variation in the load condition. The researchers believed that the solar panels needed to have a high voltage output on order to supply for the high demand of the load. Thus to satisfy the basic requirement of voltage for the system and to improve the voltage output characteristic, they had used a dc to dc converter with high voltage gain to be introduced into a stand-alone photovoltaic generation system with high efficiency. The full-bridge inverter has an important role to convert the direct current power into alternating current power source. The general work done by Rong-Jong Wai *et al.* (2008) was shown in Figure 2.2. An active sun tracker was controlled by the PWM inverter, located in the full-bridge inverter, with the aid of a digital signal processor (system controller). By this way, the active sun tracker is controlled to always facing to the sun for maximum power output.

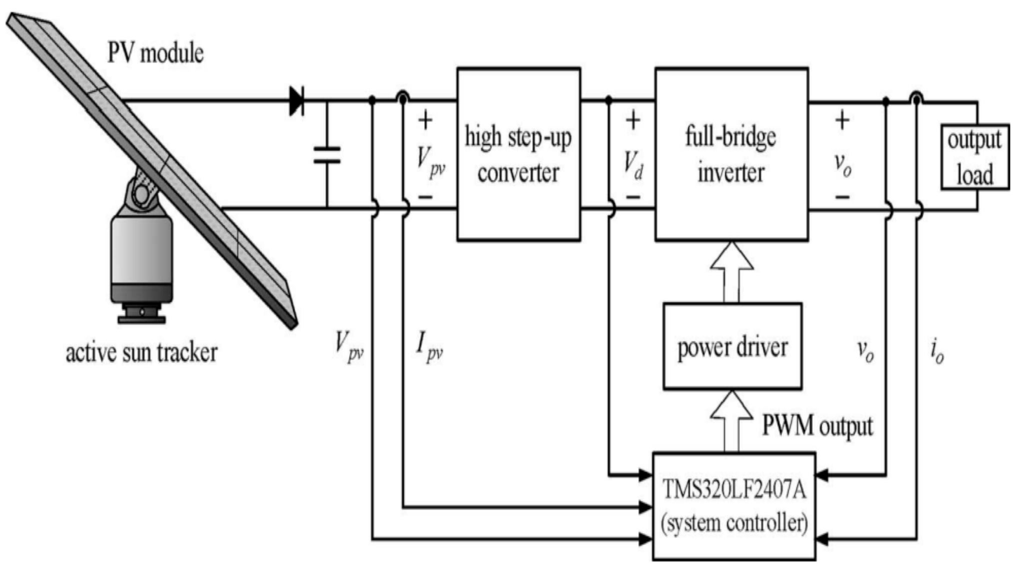

V_{pv} : Photovoltaic voltage $\qquad$ I_{pv} : Photovoltaic current

V_d : Direct current voltage $\qquad$ v_o : Output voltage

i_d : Output current

Figure 2.3: Sun tracker with high step-up converter.

2.3 Intelligent PV Modules

In the research for improving the efficiency of PV modules, Eduardo Roman *et al.* (2006) has provided discussion upon performance of two different topologies for the PV modules, namely the centralized topology and also the modular architecture. For the centralized topology, all of the PV modules are connected in series to a single inverter with a centralized MPPT. The PV modules are connected in series and they must have the same driving current. This post a problem for the system, as any one of the modules is shaded, it would be recognize as a passive load and this will in turn reduce the efficiency of the system significantly. For the modular architecture, they arranged the PV modules in series with its own MPPT. No direct connections were made between the PV modules and the dc/dc converter. Thus, this enables the PV modules to operate efficiently on its own optimal power and current, delivered all the energy to the energy storage device or load. they described that shading and mismatching can cause minor losses as well to the overall power output efficiency by the PV modules. Thus the installation of the PV modules is ideal to be at open space without nearby obstacles that will cause shading onto the PV modules.

2.4 Incident Radiation Angle Micro-sensor

The control mechanisms implemented in most of the solar tracking devices applied open-loop control scheme due to the limitation of solar sensors that are accurate to detect the position of the sun precisely. Even if the sensors are very accurate, the expensive cost for such sensors would cause a large amount of expenses for the installation and also maintenance of the devices. Jose M. Quero *et al.* (2007) introduced the micro-electromechanical system (MEMS) technologies into the application for solar tracking system sensors. The structure designed by them provides an amplification of the incident angle signal and the manufacturing process for the sensors are easy. There are two designs introduced by them .One is to apply two photodiodes which are partially covered by metal shield with aperture. The other is to use the metal shield only instead of metal shield with aperture. The researchers pointed out that the behavior of the micro-sensor is determined by the projection of the shadow onto the photodiodes. They also introduced the four quadrant sensor method which utilizes four photodiodes covered with a common shield to act as the sensor for the solar tracking system. Figure 2.4 shows the representation of the system designed by the researchers.

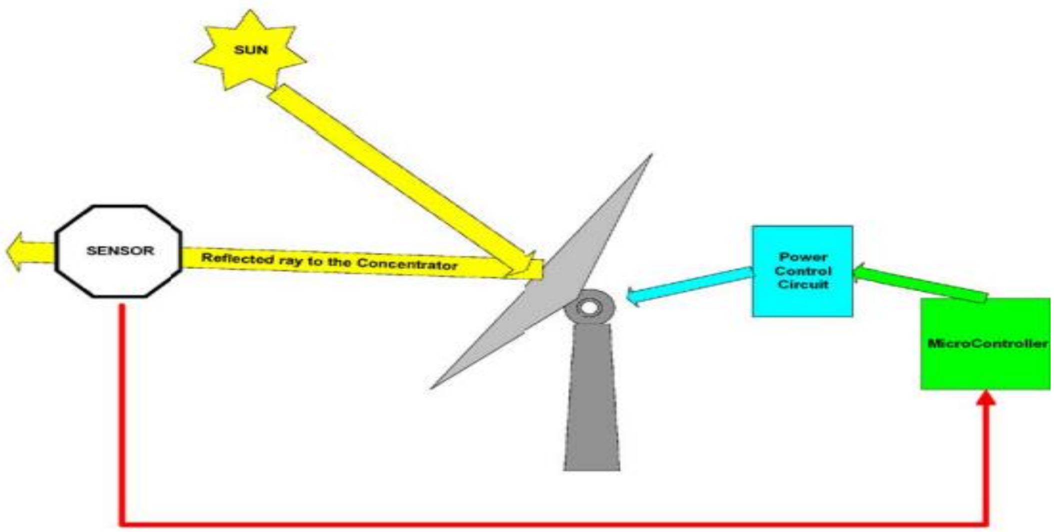

Figure 2.4: Closed loop feedback control system with incident angle sensor.

2.5 Programmable Intelligent Computer

Programmable Intelligent Controller (PIC) is one type of the components used in constructing the controller for data processing and controlling of the movement of the solar tracking system as described by A. Valan Arasu and T. Sornakumar (2007). R. Kansal and M. Singh (2009) described that the PIC works relatively faster and it provides many built-in features which other micro-controllers do not owned. In their work, they used PIC 16D877A to command the movement of the stepper motor that will rotate the solar cells towards sunshine for maximum energy output. The command pulses will be given by the PIC controller to determine the rotation of the solar cells. Work of Koh Kiong Chai *et al.* (2010) shows that PIC is used to generate the control signal for stepper motor that periodically locate for maximum radiations. In their work, they used an algorithm which forced the system to go into hibernation when the solar radiation decreases by 10% from its initial value. The techniques that they used do not require additional sensors for tracking.

CHAPTER 3

METHODOLOGY

This chapter explains in detail about the methodology of the whole system and flow of step to simulate and design of a solar tracking system that would enhance the efficiency of the solar power generation system. This chapter also describes on the circuit and device used in the project and steps for each upcoming result. The basic idea and functioning of the whole system shall be explained and discussed.

3.1 System Description

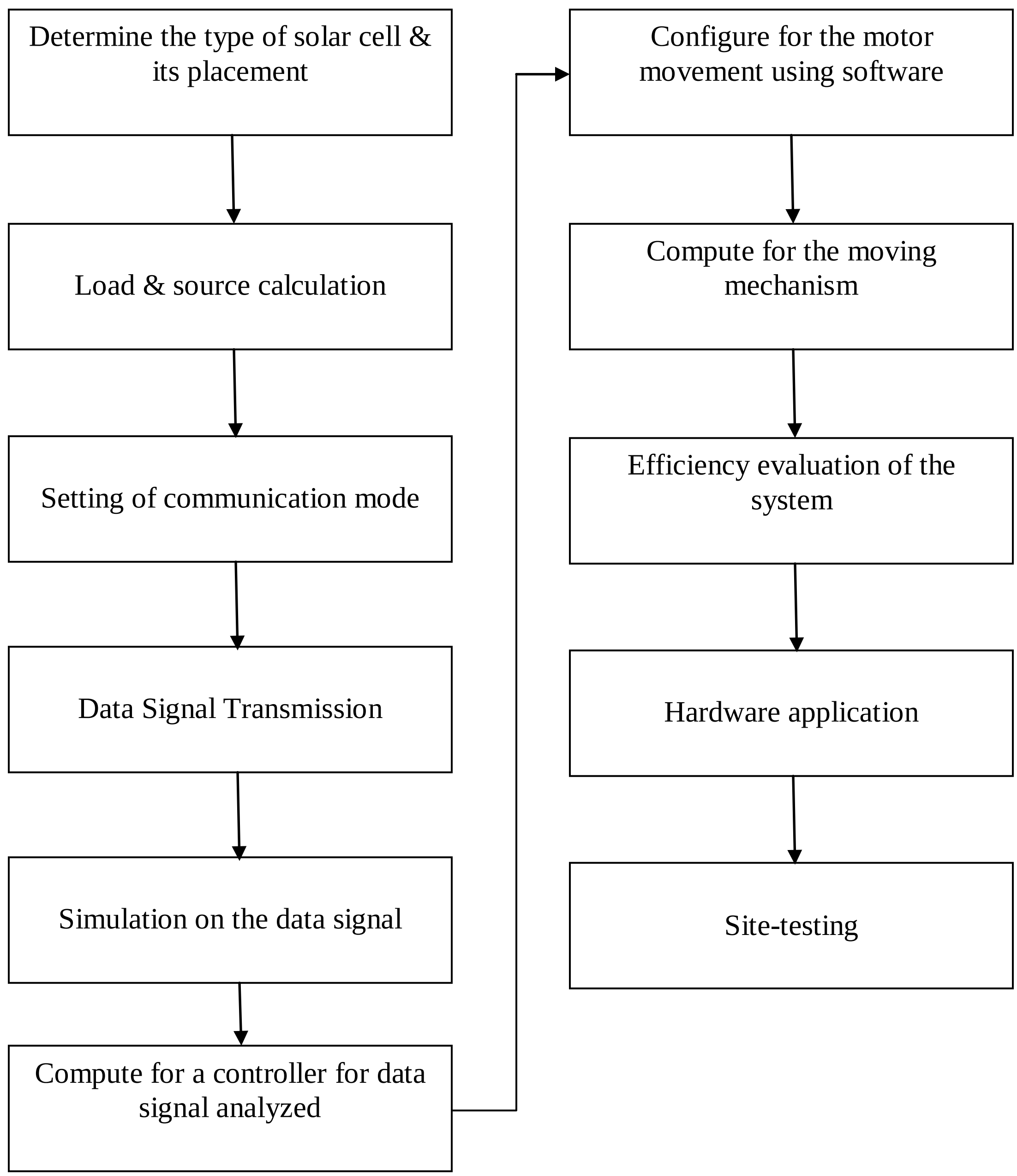

Figure 3.1: Flow Chart for the system

Firstly, the type of the solar cells or solar panel placement need to be determined. Researchs were done on the solar cells catalog for determining the type of solar cells that would be used for the system. This initial step is the most important of all, as picking up the wrong type of solar cell would greatly affect the power output efficiency of the whole system. Then the placement of the whereabouts of solar cell is determined to be in the center top of the compound parabolic concentrator. Load and source calculation is done to determine the amount of power that might be generated and used. When solar radiation falls onto the solar cells, the signal received by the sensor which is the web-camera will be send to the computer through universal serial bus (USB) wire connection with it.

Once the computer received the data, the computer software, MATLAB will simulate the signal (image of the sun) received from the web-camera and processed it. When the MATLAB software finish processing the signal, it will send in signal via USB wire through the H-bridge circuit to the stepper motor for moving the compound parabolic concentrator containing the solar cell towards the sun for maximum sun shine.

3.2 Design of the Proposed Tracking System Using MATLAB Environment

The Sun Tracking System cannot run without a software environment to control its movement. For this project, the software that will be used is MATLAB/SIMULINK. SIMULINK is a very useful tool with a wide area of application. The SIMULINK block set is used to process the data signal received from the web-camera into readable data that can be understood by the computer and provide the corresponding processes that were built in the program.

In the coming sections, each main part of the SIMULINK will be discussed in its detail function and settings, including steps on how and what values to be set for the specific block.

3.2.1 Main Tracking Model

The main tracking model of the Solar Tracking System consists of the From Video Device block is shown in Figure 3.2. The first block, From Video Device block which direct the video input from the web-camera into the SIMULINK software program. The web-camera's lens is filtered with three layers of used thin film to reduce the possible ultraviolet damage to the web-camera. This is also to provide the initial step for image processing of the image of the sun, by that way the only object that is having a high density in the visible light would be observed. The video input signal is converted into grayscale in intensity color to be conducted into the Enabled Subsystem block to start the image processing. Table 3.1 illustrates the initial settings of the Color Space Conversion Block.

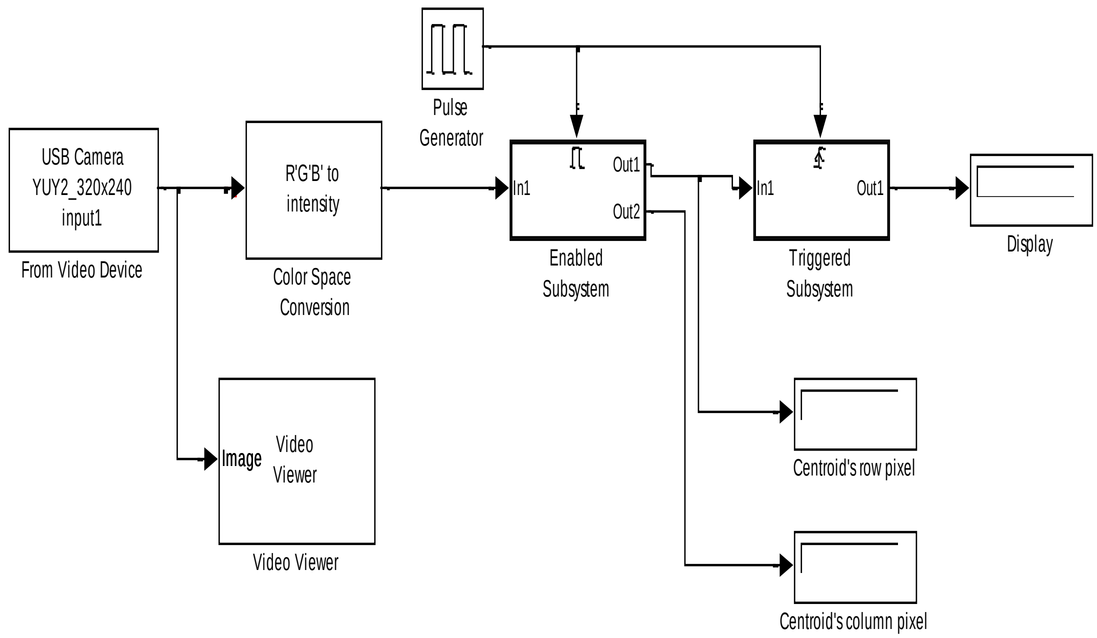

Figure 3.2: Main Tracking Model in program.

Table 3.1: Color Space Conversion block properties

Name	**Conversion Active**	**Image Ports**
Color Space Conversion	R'G'B' to intensity	One multidimensional signal

There are two main sub-system contains in the main program, namely the Enabled Subsystem (Part A) which is shown in Figure 3.3 and the Triggered Subsystem (Part B) which is shown in Figure 3.7. The Enabled Subsystem is in charge of image processing while the Triggered Subsystem is in charge of controlling motor rotation. The two Display block from Figure 3.2 will display the location of the centroid in terms of the pixels for the dimension initially set for the web-camera. The Pulse Generator block generates the pulse needed to drive the whole system in Figure 3.2 running. It is a time controlling scheme for the whole system. The initial settings of the Discrete Pulse Generator block, Display block and From Video Device block is listed in Table 3.2, Table 3.3 and Table 3.4 respectively.

Table 3.2: Discrete Pulse Generator block properties

Name	Pulse Generator
Pulse Type	Time based
Time Source	Use Simulation Time
Amplitude	1
Period	30 second
Pulse Width	50 %
Phase Delay	5 second
Sample Time	1 second

Table 3.3: Display block properties

Name	**Format**	**Decimation**	**Floating**
Centroid's column pixel	short	1	off
Centroid's row pixel	short	1	off
Display	short	1	off

Format: Specify the format for data appear.

Decimation: Specify how often to display data.

Floating: Select to use the block as a floating display.

Table 3.4: From Video Device block properties

Name	From Video Device
Device Menu	Winvideo 1 (USB camera)
ROI Position	[0 0 240 320]
Enable HWTrigger	Off
Sample Time	1/30
Output Ports Mode	One multidimensional signal
Data Type	double

The From Video Device block is placed in the main program because it is designated to be continuously functioning with real time. From Table 3.4, the value of 240 & 320 in Region of Interest (ROI) Position signifies the dimension of the image that will be captured with the web-camera. To make it simple, the ROI Position's setting in the bracket stands for [row column height width]. Meaning that with the value of 240 & 320, the dimension of the image produced shall be 240 rows of pixels X 320 columns of pixels. In the coming section, explanation on the Enabled Subsystem will be discussed.

3.2.2 Enabled Subsystem (Part A) Model

Once all the blocks in Chapter 3.1.1 have been set, the content of Enabled Subsystem (Part A) can now be design. The main function of this subsystem block is to carry out the image processing and image analyzing. There are three main processes that are included in this subsystem, namely Image Enhancement (Part C), Morphology Operation (Part D) and Marking Process (Part E). Figure 3.3 shows the Enabled Subsystem model for the system.

Referring to Figure 3.3, after double clicking into the Enabled Subsystem, the first block to be observed is the enable clock. It continuously enables the subsystem to continue propagating signal from input to the output. Part C, Part D and Part E will be explained in the coming sections. The Insert Text block draws formatted text or numbers on an image or video stream. The Variable Selector block extracts a subset of rows or columns from the M-by-N input matrix which is the signal at each input port. The Select parameter in the Variable Selector block needs to be set. When the Select parameter is set to Rows, the Variable Selector block extracts rows from each input matrix, while if the Select parameter is set to Columns, the block extracts columns. The initial settings for these blocks are shown in Table 3.5 and Table 3.6.

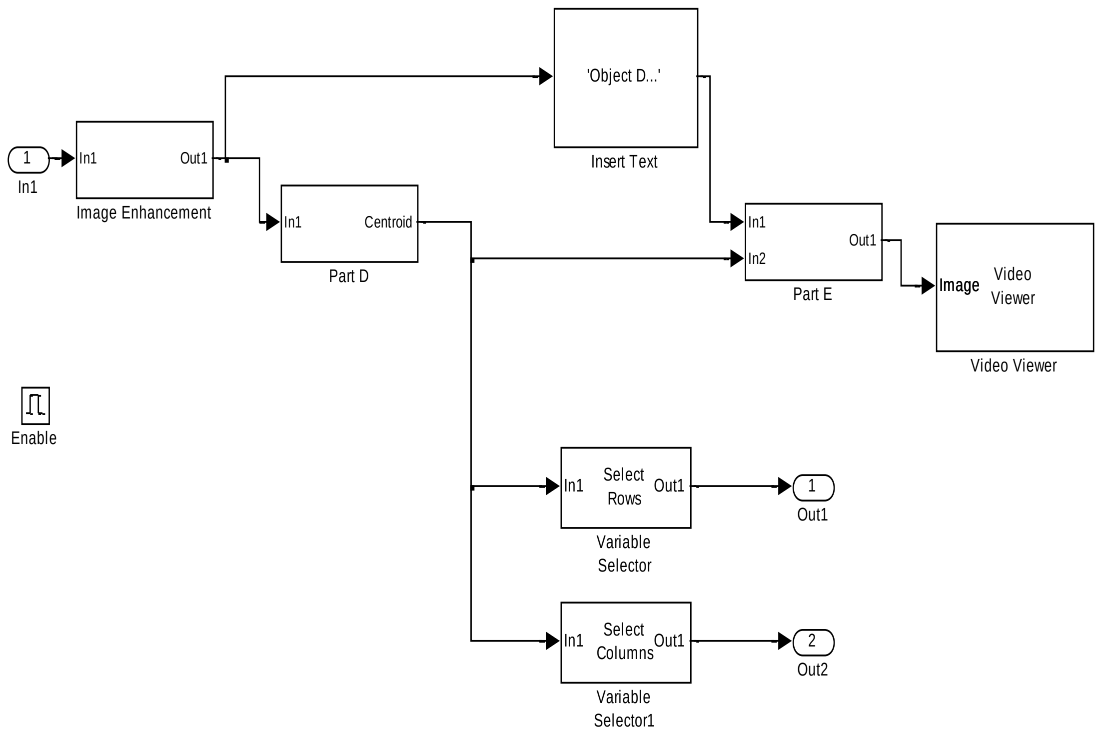

Figure 3.3: Enabled Subsystem model for the system

Table 3.5: Insert Text Block Properties

Name	Insert Text
The Text	'Object Detected'
Font Face	Lucida Sans Regular
Block Font Size	12
Anti Aliased	On

Get Text Loc From	Specify via dialog
Text Loc	[80 100]
Get Text Color From	Specify via dialog
Text Color	[0 0 0]
Get Text Opacity From	Specify via dialog
Text Opacity	1.0
Image Ports	One multidimensional signal
Is Input Transposed	off

Table 3.6: Variable Selector block properties

Name	Variable Selector	Variable Selector 1
Num Inputs	1	1
Rows Or Cols	Rows	Columns
Idx Mode	Fixed	Fixed
Elements	[1 3]	[1 3]
Zer One Idx Mode	Zero-based	Zero-based
Errmode	Clip Index	Clip Index
Fill Mode	On	On
Fill Values	-1	-1

3.2.3 Image Enhancement (Part C) Model

Figure 3.4 shows the Image Enhancement (Part C) model for the system. There are three blocks in this part, Gamma Correction block, Median Filter block and Video Viewer block. The main function of this part is to enhance the image received into clearer and noise-free image to be processed further in the other parts. This step is important to enable the system to obtain a clear signal to detect the object- sun. The Video Viewer block outputs the image after processed to be viewed in another window in the computer. The Gamma Correction block applies gamma correction upon the image received from the web-camera. The Median Filter block replaces the central value of the M-by-N matrix, which is the data signal in process, with its median value. This is to avoid the image after enhancement having the center of image with the most intensity and make the image after processed become uneven in its intensity distribution. The initial settings for these blocks are shown in Table 3.7 and Table 3.8. The Video Viewer block does not need to be specifically set again as its only function is to project the image processed.

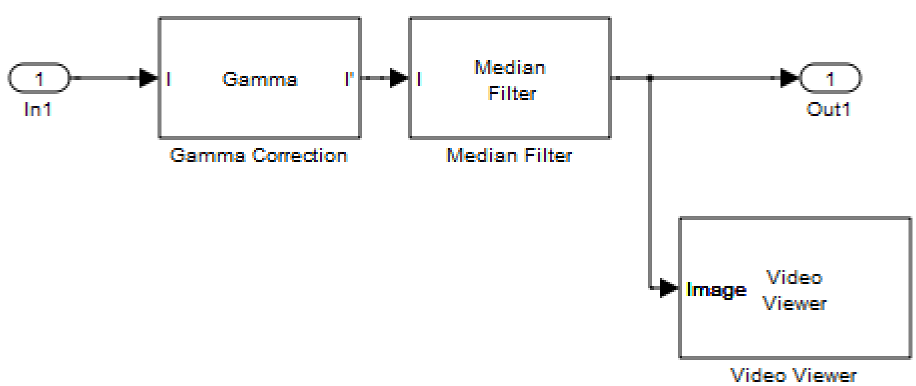

Figure 3.4: Image Enhancement Model for the system

Table 3.7: Gamma Correction Block Properties

Name	Gamma Correction
Operation	Gamma
Gamma	2.2
Linear Segment	On
Break Point	0.018

Table 3.8: Median Filter Block Properties

Name	Median Filter
Nghbood	[3 3]
Out size	Same as input port I
Pad Type	Constant
Pad Src	Specify via dialog
Pad Val	0
Output Mode	Same as input
Output Word Length	16
Output Frac Length	15
Axxum Mode	same as input
Axxum Word length	32

Accum Frac Length	30
Prod Output Mode	Same as input
Prod Output Word Length	32
Prod Output Frac Length	30
Rounding Mode	Floor
Overflow Mode	Off
Lock Scale	Off

3.2.4 Morphology Operation (Part D) Model

Figure 3.5 shows the Morphology Operation (Part D) for the system. There are four blocks here which account for the threshold process, morphological operation and also blob analysis. For threshold process, the Autothreshold block is used. This block functions to convert the image after enhancement process into black and white color image, which means that the binary image will be transform into binary image. Binary image only contains 2 values for its data, either one (1) or zero (0). The value one is the place whereby the object presents and is represented by white color, while the value zero is the place whereby the object absent and is represented by black color. After this is done, the morphological process which consists of Erosion block and also Dilation block is proceed. The Erosion block slides the structuring element over an image, finds the local minima and creates the output matrix from them. Meanwhile, Dilation block rotates the structuring element by 180 degrees and slides it over the image. It would creates the output matrix once if finds the local maxima.

The Display block will display the number of object found in the image processed. The Blob Analysis block calculates the statistics for the labeled regions in the binary image produced by the Autothreshold block. The centroid of the image (sun) is found by using this block. The Blob Analysis block functions using the pixel coordinates, whereby the first component row (r) increase downward while the second component column (c) increases to the right. For this system, the range of the value for the rows is 0 to 240 and for columns is 0 to 320. The initial settings for these blocks are shown in Table 3.9, Table 3.10, Table 3.11 and also Table 3.12.

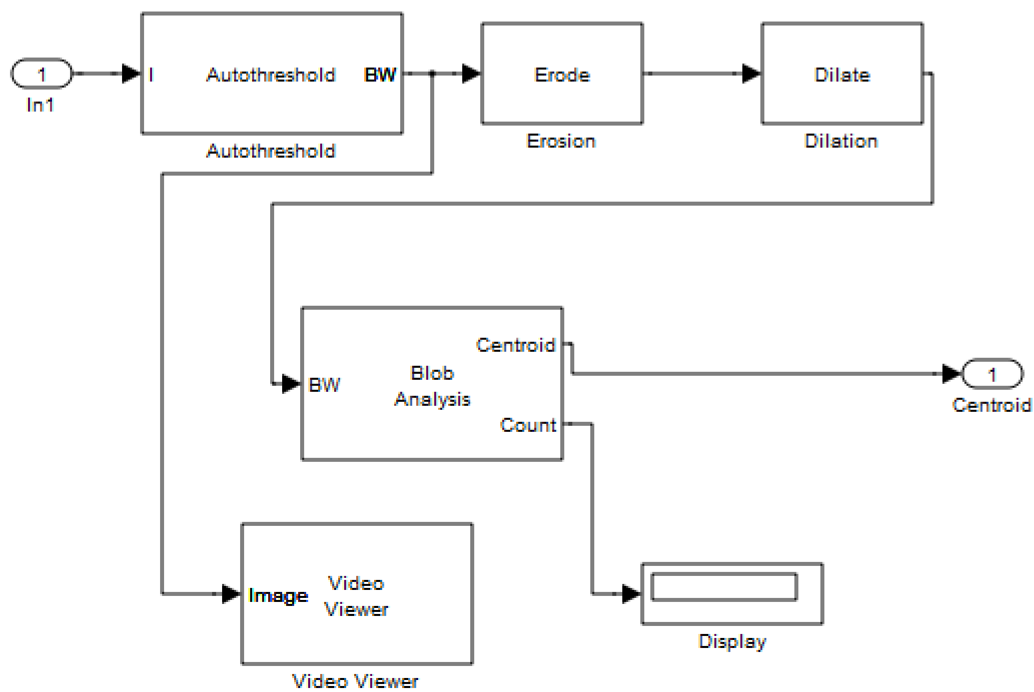

Figure 3.5: Morphological Operation model for the system

Table 3.9: Autothreshold block properties

Name	Autothreshold
Operator	>
Thresh Out	Off
Eff Metric Out	Off
User Defined Range	Off
Umin	0
Umax	255
Out Of Rng Opt	Ward and saturate
Scale Threshold	Off
Scale Factor	1
P1mode	Specify word length
P1word Length	32
P1frac Length	30
A1mode	Same as product 1
A1word Length	32
Alfrac Length	30
P2mode	Specify word length
P1word Length	32
P2 Frac Length	22

A2mode	Same as product 2
A2word Length	22
P3mode	Specify word length
P3word Length	32
P3frac Length	14
A3mode	Same as product 3
A3word Length	14
P4mode	Binary point scaling
P4word Length	32
P4frac Length	15
A4mode	Same as product 4
A4word Length	16
A4frac Length	4
Q1 Mode	Specify word length
Q1 Word Length	32
Q1frac Length	16
Emmode	Specify word length
Emword Length	16
Emfrac Length	14
Rounding Mode	Floor

Overflow Mode	Off
Lock Scale	off

Table 3.10: Dilation block properties

Name	Dilation
Nhoodsrc	Specify via dialog
Strel	[1 1; 1 1]

Table 3.11: Erosion block properties

Name	Erosion
Nhoodsrc	Specify via dialog
Strel	Strel('square',4)

Table 3.12: Blob Analysis block properties

Name	Part D
Area	Off
Centroid	Off

Bbox	On
Major Axis	Off
Minor Axis	Off
Angle	Off
Eccentricity	Off
Equiv Diameter Sq	Off
Extent	Off
Perimeter	Off
Max Blobx	50
Warn If Num Blobs Exceeded	On
Is Count	On
Use Min Area	Off
Min Area	0
Use Max Area	Off
Max Area	Inf
Exclude Border Blob	Off
Is Out Var Dim	Off
Is Fill	On
Fill Valued	-1
Conn	8

Is Label	Off
Output Mode	Binary point scaling
Output Word Length	32
Output Frac Length	16
Memory Mode	Same as product output
Memory Word Length	32
Memory Frac Length	16
First Coeff Mode	Binary point scaling
First Coeff Word Length	16
First Coeff Frac Length	14
Second Coeff Mode	Binary point scaling
Second Coeff Word Length	32
Second Coeff Frac Length	16
Accum Mode	Binary point scaling
Prod Outout Mode	Binary point scaling
Rounding Mode	Floor
Overflow Mode	Off
Lock Scale	Off

3.2.5 Marking Process (Part E) Model

The only purpose of this part is to mark the centroid of the object that will appear in the image received and processed after the morphological operation (Part D). For any object present, it will be mark with a circle for easier identification of the number of the object. Figure 3.6 shows the Marking Process (Part E) model. The initial setting for the Draw Markers block is shown in Table 3.13.

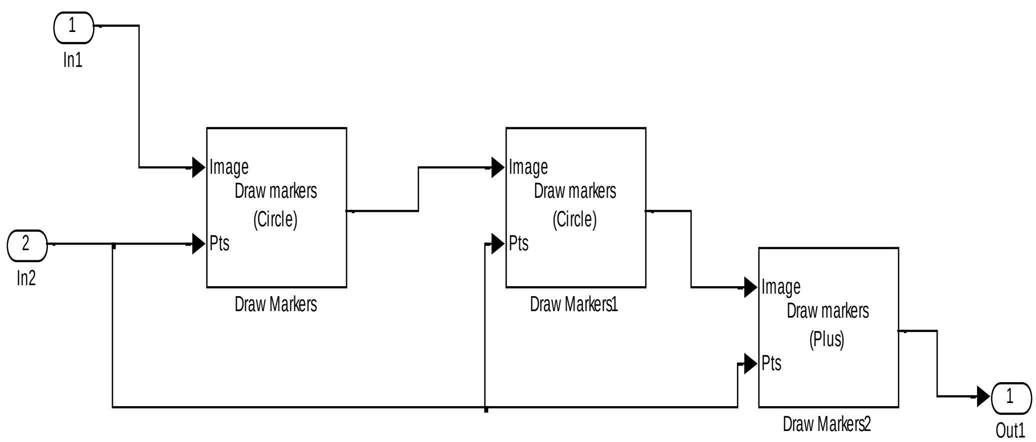

Figure 3.6: Marking Process (Part E) model in the system

Table 3.13: Draw Markers block properties

Name	Draw markers	Draw markers1	Draw markers2
Shape	Circle	Circle	Plus
Size	3	3	3

Fill	Off	Off	Off
Fill Clr Source	Specify via dialog	Specify via dialog	Specify via dialog
Display	Black	Black	Black
Intensity	155	155	155
Color	[200 120 50]	[200 120 50]	[200 120 50]
Opacity	1	1	1
Viewpoint	Entire image	Entire image	Entire image
Antialiasing	Off	Off	Off
Image Ports	One multidimensional signal	One multidimensional signal	One multidimensional signal
Accum Mode	Same as product output	Same as product output	Same as product output
Accum Word Length	32	32	32
Accum Frac Length	14	14	14
Prod Output Mode	Binary point scaling	Binary point scaling	Binary point scaling
Prod Output Word Length	32	32	32
Prod Output Frac Length	14	14	14

Memory Mode	Specify word length	Specify word length	Specify word length
Memory Word Length	16	16	16
Memory Frac Length	15	15	15
Rounding Mode	Floor	Floor	Floor
Overflow Mode	Off	Off	Off
Lock Scale	Off	Off	Off

3.2.6 Triggered Subsystem (Part B) Model

Figure 3.7 shows the Triggered Subsystem (Part B) model used in the system. This subsystem received signals from two different sources. One is the pulse generator block and also data signal from Part A. Part B will be triggered to function only when it received the data from both the sources mentioned. This part will associate the signal received from the previous parts and propagate the command to the sound card in the computer to conduct further signal to the H-bridge circuit to move the stepper motor accordingly towards the sun.

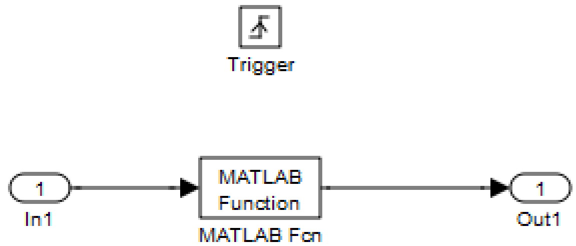

Figure 3.7: Triggered Subsystem model in the system

3.3 Hardware Implementation

The interfacing between the software and hardware can be done by using the sound card in the computer as the output channel. The signals from the sound card produced are made out of positive and negative signal (the sound card needs to be defined in the MATLAB to be used for output channel in series or parallel port). A representation of the H-bridge circuit connected with the system is shown in Figure 3.8. Through the H-bridge circuit which is made out of four MOSFET (IRF 530), the positive signal will generate the forward rotation command to the stepper motor while the negative signal will generate the reverse rotation command to the stepper motor. Since only one stepper motor will be used, this stepper will carry out the tilt rotation of the solar tracking system.

A cooking wok wrapped with aluminium foil is used to represent the compound parabolic concentrator (CPC) in this project. The solar cell chosen need to be of small scale to be able to fit into the CPC. Thus the solar cell chosen is the 2.4 V / 0.5 W Mono-Crystalline solar cell. The image of the solar cell used is shown in Figure 3.9. This solar cell will be mounted below the web-camera facing down towards the CPC. The web-camera will be placed on above the CPC held by two light weight wooden sticks. The choice of using wooden sticks to support for the web-camera is due to the small and thin in shapes which do not cause much shading to CPC. Solar charge controller with specification range from 5V to 12V is shown in Figure 3.10. A 12V solar rechargeable battery with specification of 2.3 Ah is used as the energy storage and the power source to drive the H-bridge circuit and also the stepper motor. The image of the solar rechargeable battery is shown in Figure 3.11.

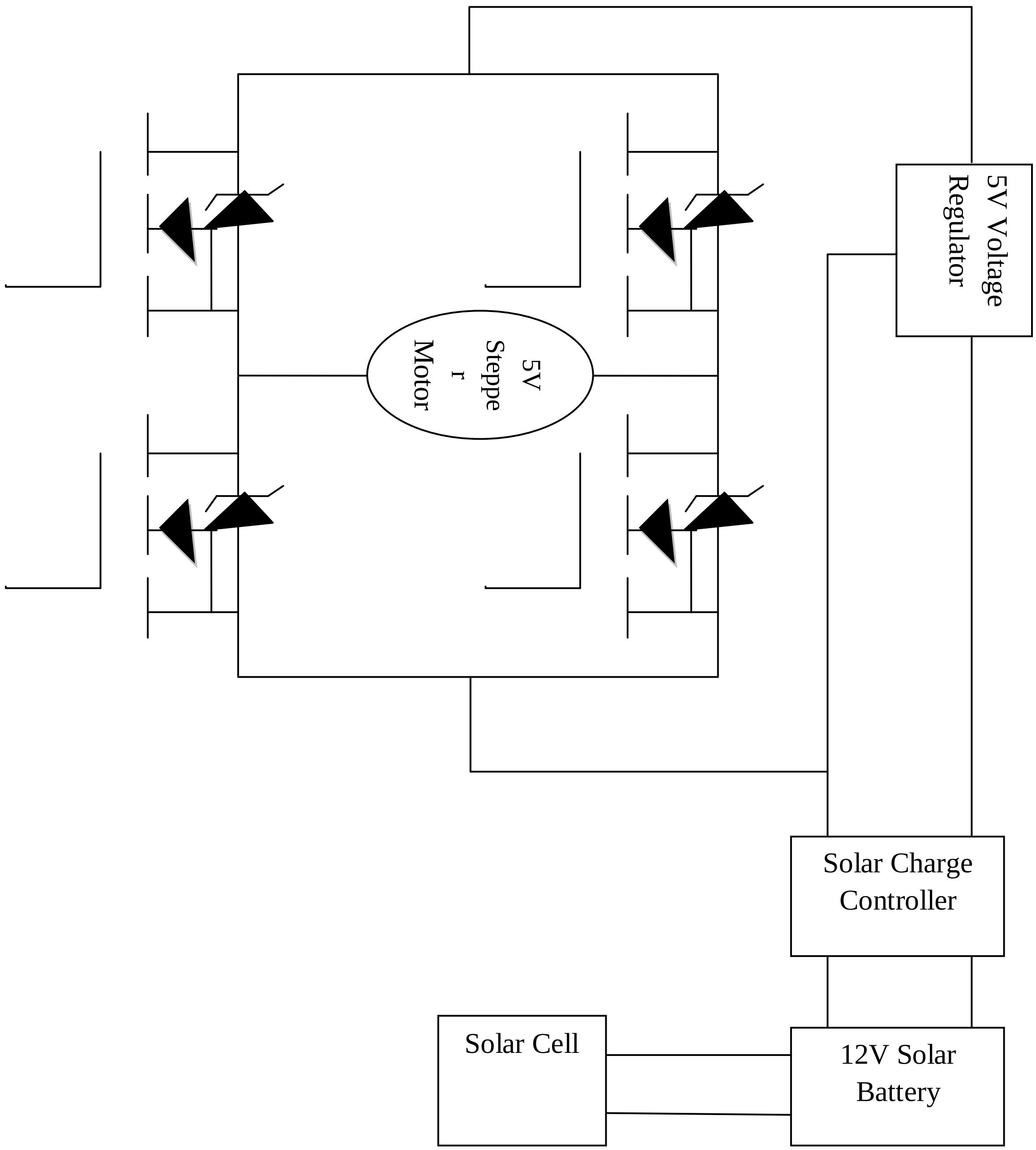

Figure 3.8: H-bridge circuit with MOSFET IRF530

Figure 3.9: Solar Cell 2.4V / 0.5W

Figure 3.10: Solar Charge Controller 5V-12V

Figure 3.11: Solar rechargeable battery 12 V / 2.3 Ah

Figure 3.12: CPC with Solar Cell & Web-Camera Mounted on it.

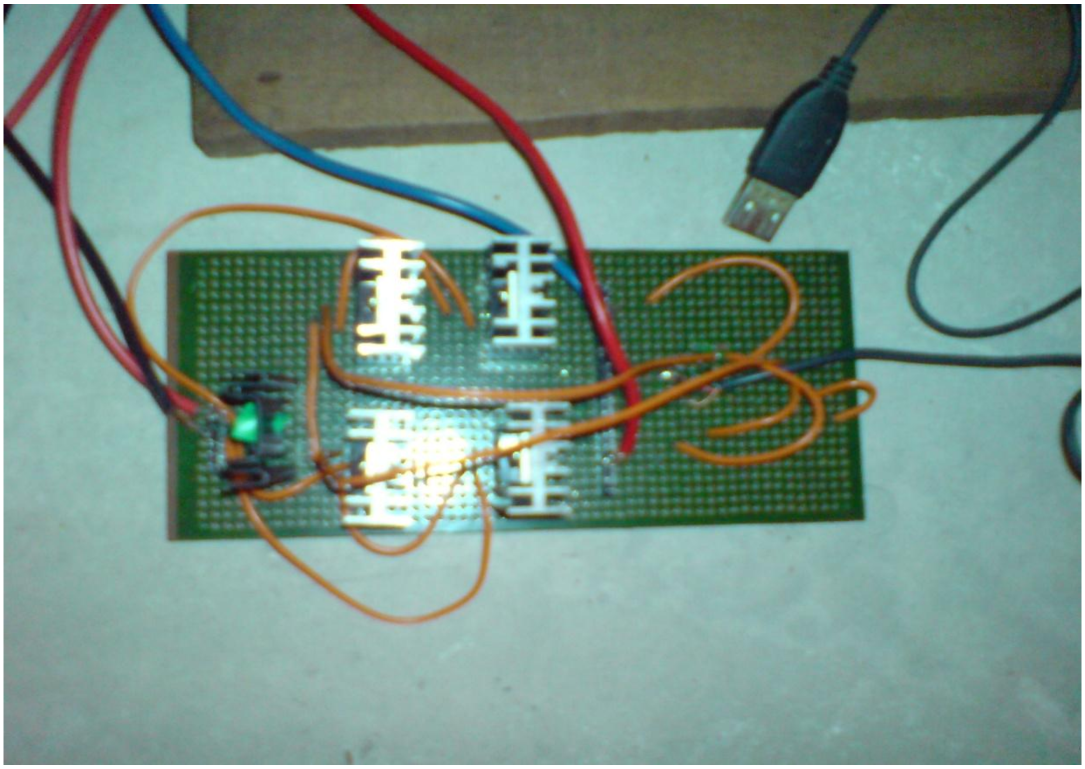

Figure 3.13: Half-Bridge Driving Circuit.

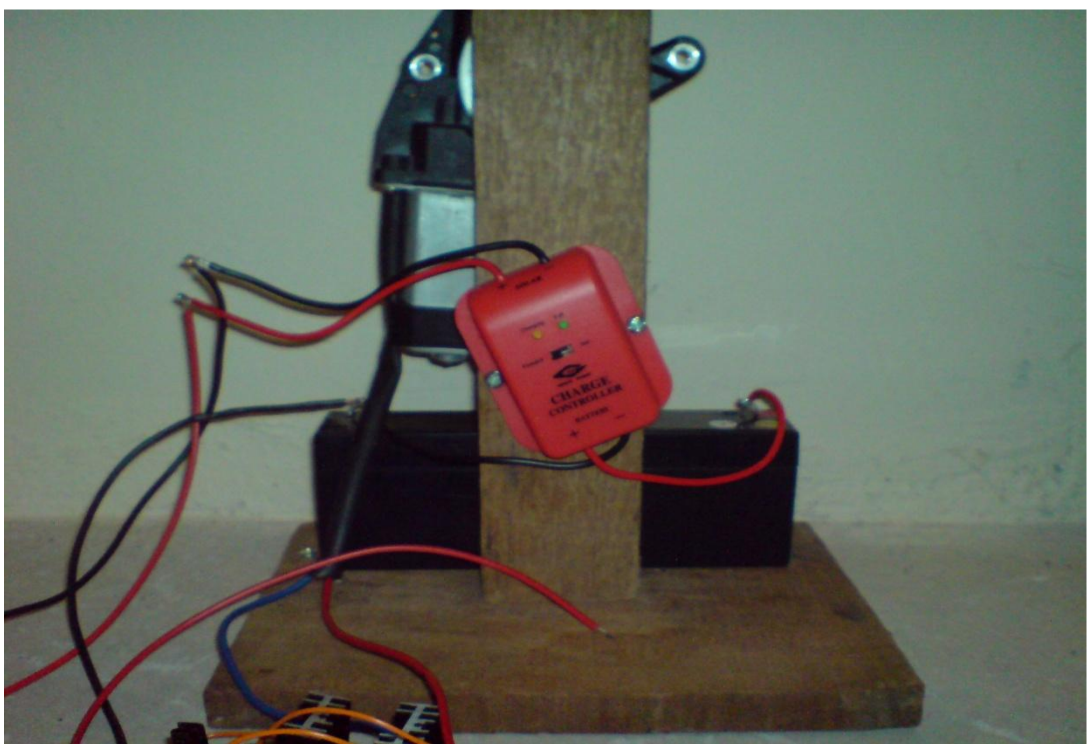

Figure 3.14: Back View of System (Solar Charge Controller)

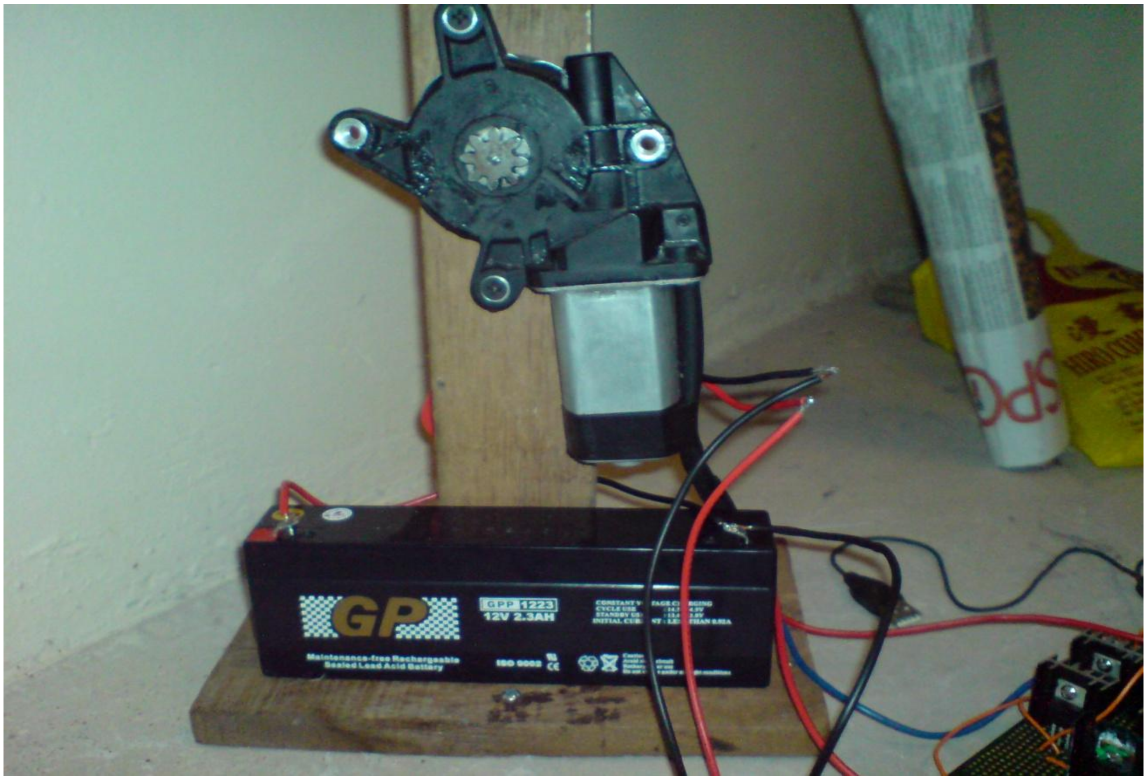

Figure 3.15: Front View of System (Stepper Motor & Solar Battery)

3.4 Mathematical Consideration

For a solar power generation system, some basic formula need to be practice and used before any installation of solar photovoltaic system. These formulas have been practiced by K. K. Tse *et al.* (2004). The formulas are shown below:

$$V_{ef}\,(\%) = \frac{V_{sc}}{V_{\max}}\, X100\% \tag{1}$$

X : Times

V_{ef} : Voltage Efficiency

V_{sc} : Voltage Received by Solar Cell

$V_{\max}$: Maximum Voltage Specification of the Solar Cell.

$$M_n(unit) = \frac{P_r(kW/day)}{P_s(kW/day)XB_{cef}(\%)} \tag{2}$$

kW/day : kilo Watt per day

M_n : Minimum Number of Solar Modules

P_r : Daily Power Requirement

P_s : Daily Output of one Solar Module

B_{cef} : Battery Charging Efficiency

$$C_u(Ah) = \frac{P_r(kW/day)XD_s(days)}{12(V)} \tag{3}$$

Ah : Ampere-hour

D_s : Days of Storage for Battery

C_u : Total Usable Capacity of battery needed for a 12 V system

$$M_s = \frac{C_u(Ah)}{C_f(Ah)XD_{dc}(\%)} \tag{4}$$

M_s : Minimum Number of Batteries needed for a 12 V system

C_f : Full Capacity of a Solar Battery

D_{dc} : Depth of Cycle for Discharging a Battery

CHAPTER 4

RESULT AND DISCUSSION

This chapter will focus on discussion of the result of the simulation and also the result of the voltage output obtained from the solar cell. The discussion will also discuss about the overall reputation of the system proposed and evaluate the specifications of the components chosen.

4.1 Software Simulation

The system utilizes MATLAB/SIMULINK in order to carry out the image processing operation for the solar tracking system. The blocks used for the program to control the tracking process of the system are mostly obtained from the video & image processing block set. Thus, much of the result will be in shown in terms of diagrams / figures to prove that the data signal was received, processed and analyzed successfully by the model simulated. Achieving the simulation result is one of the objectives for this project.

Referring to Figure 3.2 in chapter 3.1.1, where both of the Display blocks named as Centroid's Row Pixel Number and also the Centroid's Column Pixel Number before the simulation do not contain any value inside the block. After the simulation started and the model has successfully detect and determined the position of the sun, the values of the centroid of the image of the sun received by the web-camera for that instance has been found. Figure 4.1 shows the displayed result for the position of centroid for the image of the sun for that instance and this result is also tabulated in Table 4.1.

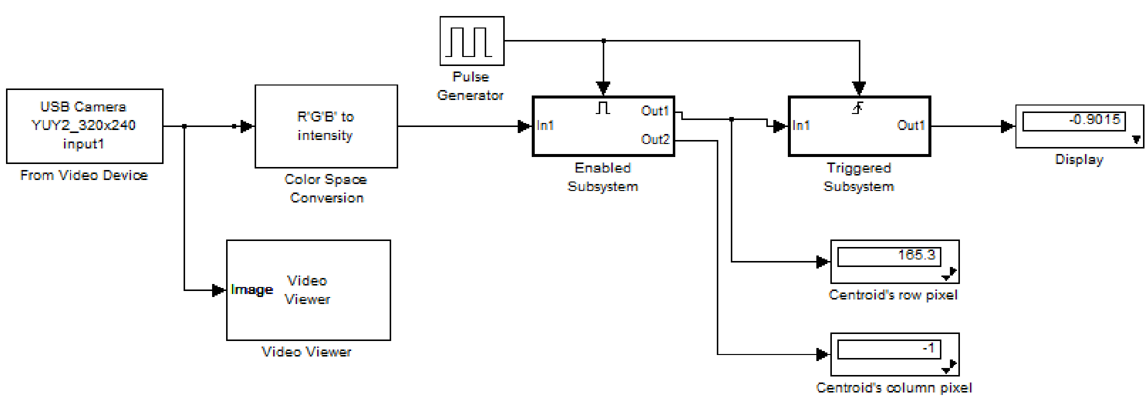

Figure 4.1: Centroid's position values displayed.

Table 4.1: Centroid's Pixel Number

Centroid's Row Pixel Number	165.3
Centroid's Column Pixel Number	-1

The values of Centroid are displayed in the Display blocks. For that instance whereby the program is running and the sun is able to be tracked, the centroid has been located in the middle of the sun image received by the web-camera. The numbers displayed are showing the location of the centroid in the image captured with the web-camera that is initially set to the dimension of 240 X 320 pixels. This is confirmed by referring back to Table 3.4, row number three, whereby the initial setting for the height of the web-camera image is 240 rows and width of the web-camera image is 320 columns.

The original sun image accepted by the web-camera is directed to the Video Viewer block in the main tracking model in Figure 3.2. The purpose of this block is to make sure that input signal from the web-camera is propagated correctly to the next block. The image received by the web-camera is shown in Figure 4.2.

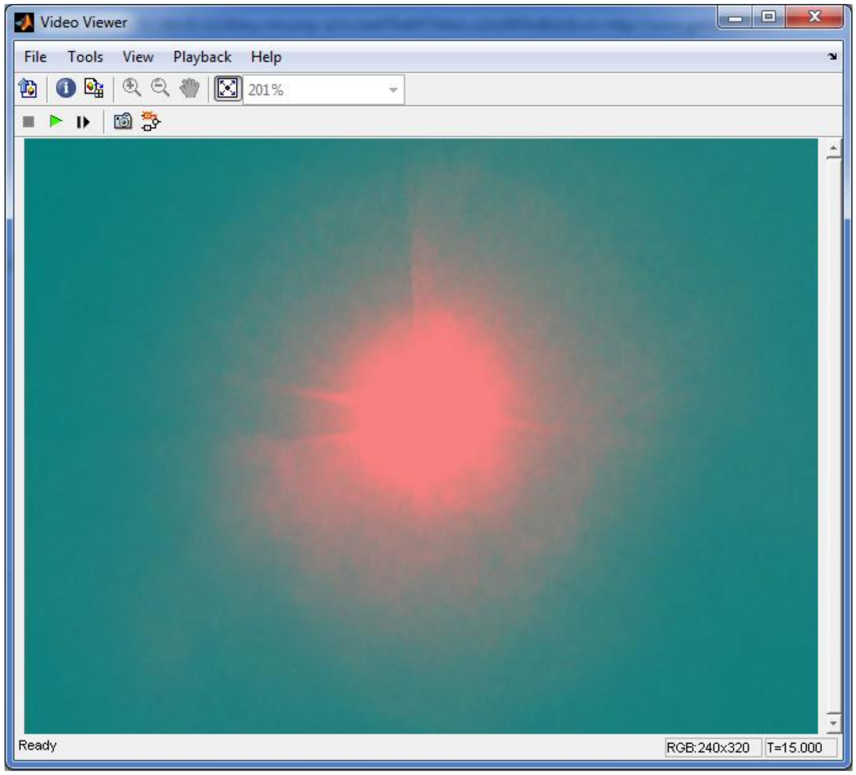

Figure 4.2: Original Sun Image by Web-camera.

For this section, the outputs from the Variable Selector blocks (Figure 3.3) have been directed out to be displayed in the Display blocks in Figure 3.2, which are the Centroid's Row Pixel and also the Centroid's Column Pixel. Thus the output in the Enabled Subsystem is the image of the sun after it has gone through three main processes, namely Image Enhancement, Morphology Operation and Marking Process. In the mean time, the image produced has been enhanced into clearer image, converted from intensity (degree of the strength of light) image into binary (consisting of number system with two as its base) image and marked its centroid with circle.

The output image of the video viewer contains within this Enabled Subsystem is shown as Figure 4.3. This figure shows that the Enabled Subsystem has successfully received the data signal from the web-camera. The image has been processed and analyzed to show that the system has successfully detect the only one object that this project desired to track, which is the sun.

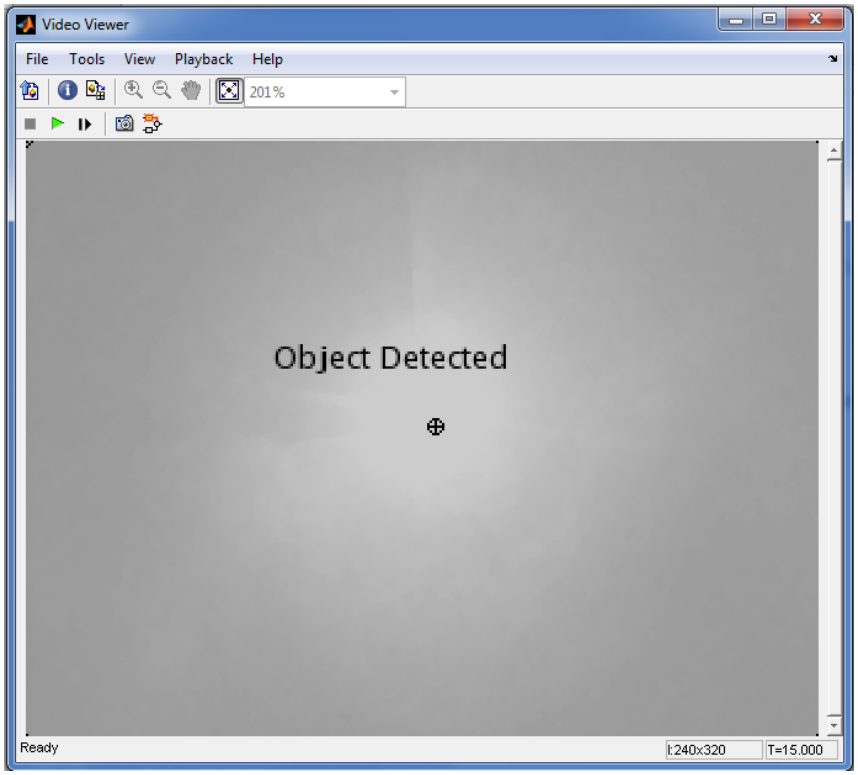

Figure 4.3: Sun Image after Enhancement, Morphology & Marking Process.

The enhancement of image is carried out to improve the image received from the web-camera (Figure 4.2) into clearer image for better efficiency of the system. The image as shown in Figure 4.2 undergo Gamma Correction block and Median Filter Block in Figure 3.4 to produce a new image with less noise. At the same time, without significantly reducing the sharpness of image, the image is processed and filter into the image shown in Figure 4.4.

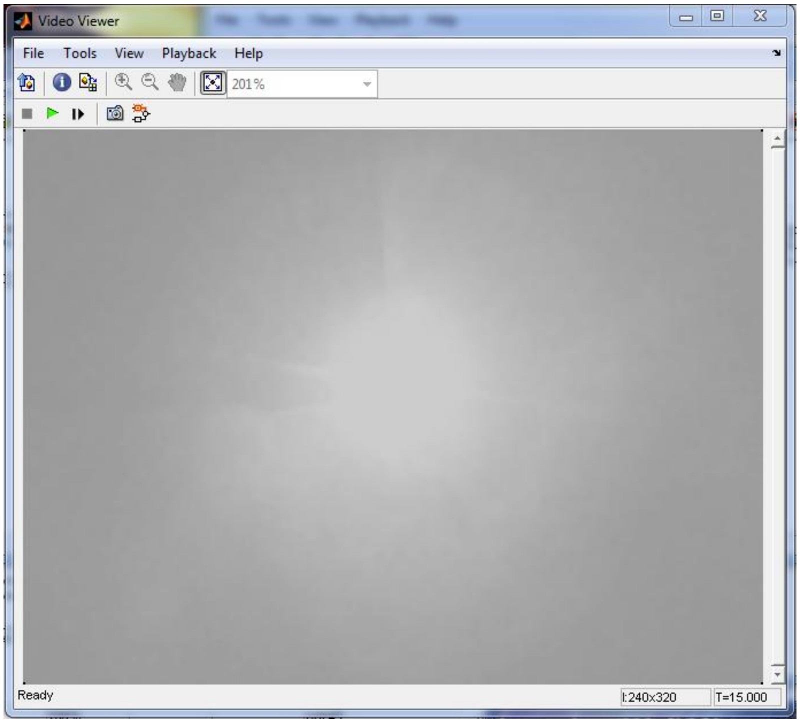

Figure 4.4: Sun Image in Image Enhancement Subsystem.

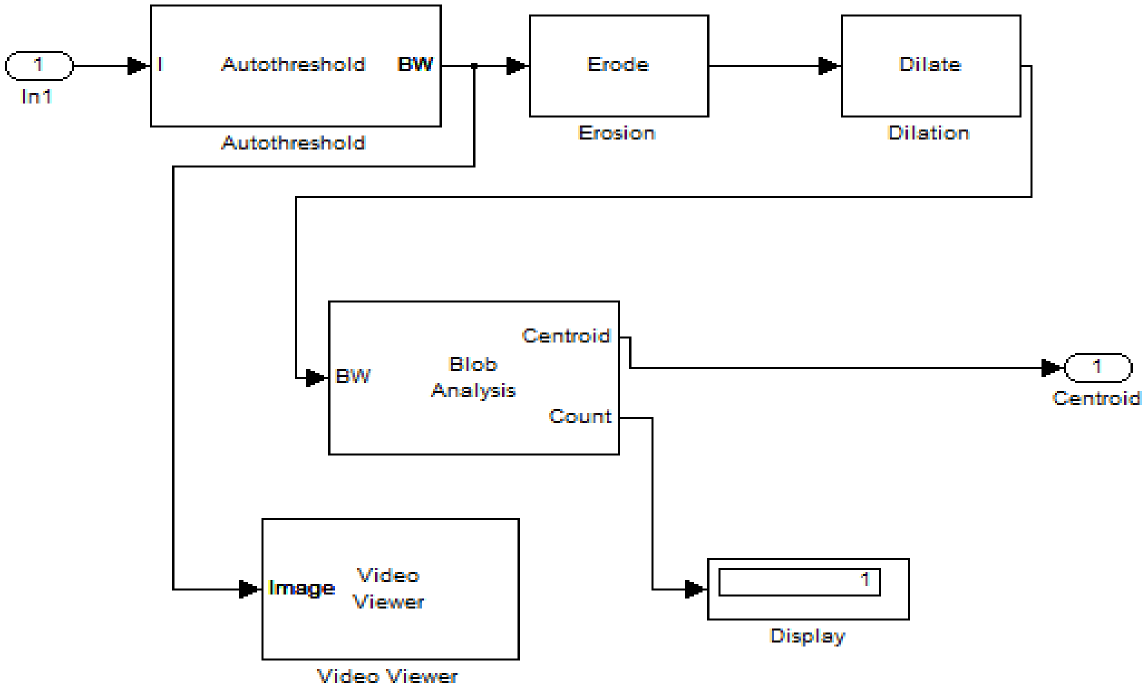

Figure 4.5: Morphological Subsystem with Number of Object Detected Displayed.

The Display block in Figure 4.5 shows the number of object detected is one. This is due to the high intensity of the sun image in Figure 4.4 which had enhances the quality of the image received for the following process to convert it into binary image. This intensified image of the sun is converted into binary image which only consists of black and white color. The background of the image is all zero-based (0) pixels and therefore it is black in color. The object detected will be marked as having the value of one (1) and thus it will turn out to be white in color in binary image. The sun image in Figure 4.5 is a group of intensified and centralized pixels (smallest addressable screen element) in the middle. And so therefore, Figure 4.6 appears as a group of white image (object) central in the middle of the black background. This is the reason why the program can carry out the solar tracking purpose, because it needs to track the one and only object that it detects with the most intensified binary values in its image.

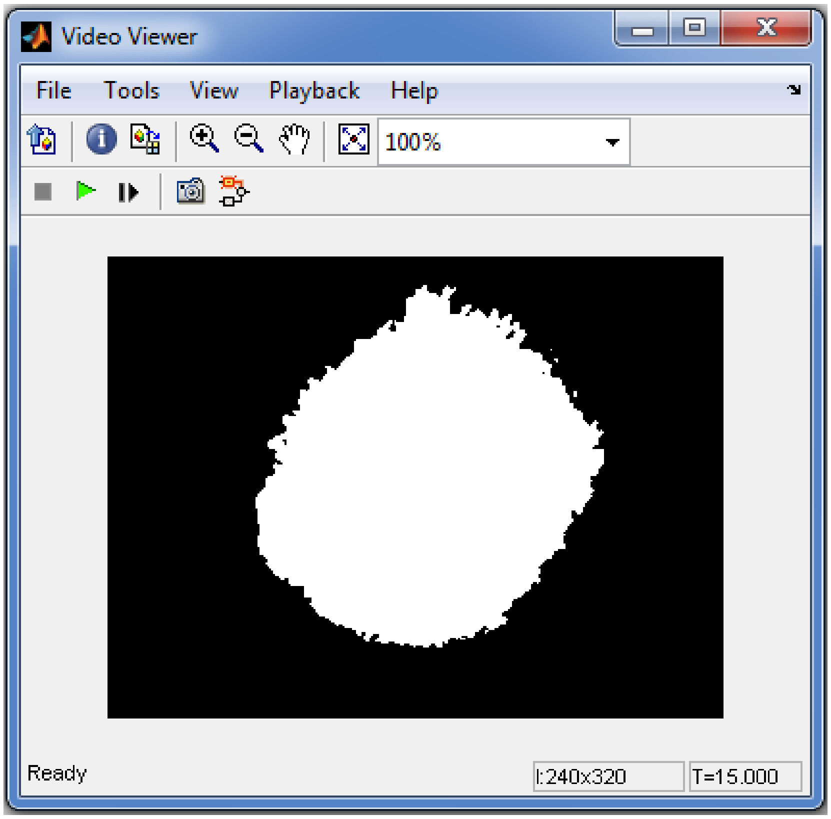

Figure 4.6: Sun Image after Binary Conversion Process.

4.2 Voltage Efficiency

The voltage received by directing the CPC perpendicular to the sun with the solar cell mounted on it towards the sunlight, is compared with the voltage received by not directing the CPC towards the sunlight. This is to represent the comparison between the voltage received by movements of the stepper motor to move the CPC towards the sunlight when it successfully tracked the sun and the static non-moving solar cell.

Table 4.2: Voltage received by utilizing solar tracking based on web-camera

Time of Day	**Voltage Received, V**	**Charging Current, mA**	**Hour Angle for Northern Hemisphere, °**	**Cell Surface Temperature, ℃**	**Voltage Efficiency (%)**
11:30am	1.2	5.8	- 7.5	31.4	50.0
12:00pm	1.3	5.5	0	31.0	54.2
12:30pm	1.3	6.0	7.5	30.6	54.2
1:00pm	1.2	6.1	15	31.2	50.0
1:30pm	1.1	6.6	22.5	31.9	45.8
2:00pm	0.9	6.0	30	32.5	37.5
2:30pm	1.1	5.9	37.5	32.4	45.8
3:00pm	1.0	5.5	45	31.8	41.7
3:30pm	1.2	5.4	52.5	31.6	50.0
4:00pm	1.0	5.7	60	32.3	41.7
4:30pm	1.1	5.3	67.5	33.1	45.8

Table 4.3: Voltage received without utilizing solar tracking based on web-camera

Time of Day	**Voltage Received, V**	**Charging Current, mA**	**Angle of the sun's position, °**	**Cell Surface Temperature, ℃**	**Voltage Efficiency (%)**
11:30am	1.0	5.7	- 7.5	31.2	41.7
12:00pm	1.2	5.6	0	31.3	50.0
12:30pm	1.3	5.9	7.5	30.2	54.2
1:00pm	1.1	6.1	15	30.8	45.8
1:30pm	0.9	6.2	22.5	32.0	37.5
2:00pm	0.7	6.0	30	32.5	29.2
2:30pm	0.9	5.8	37.5	31.9	37.5
3:00pm	0.8	5.6	45	32.0	33.3
3:30pm	1.0	5.5	52.5	31.6	41.7
4:00pm	1.0	5.6	60	32.1	41.7
4:30pm	0.8	5.4	67.5	32.8	33.3

From Table 4.2 and Table 4.3, it can be concluded that by directing the CPC containing the solar cell perpendicular towards the sun's position will increase the overall efficiency of the system. Investigating the data in Table 4.2 and Table 4.3, there is a sudden drop of voltage generated by the solar cell. This is due to the cloudy condition for that certain moment of the day. The voltage received is at its peak around 11:30pm to 1:00pm due to the position of the sun which is directly above in the middle of the sky. This causes the direct radiation to the solar cell to be at its maximum radiation for that area.

4.3 Hardware Result

The hardware results for the sun tracking system are illustrated in Table 4.4. Basically the result can be analyzed in two aspects, which are the signs of the values and the magnitude of the values. The positive controlling signal will be used to drive for the forward rotation of the stepper motor, while the negative controlling signal will be used to drive for the backward rotation of the stepper motor. Whereas for the effect of magnitude, the larger the values of the controlling signal, the further the stepper motor will be drive for the direction designated by the signs of the controlling signal.

Table 4.4: Effect of Signs of Controlling Signal

Simulating Signal	Hardware Response
Negative	Backward Rotation
Positive	Forward Rotation

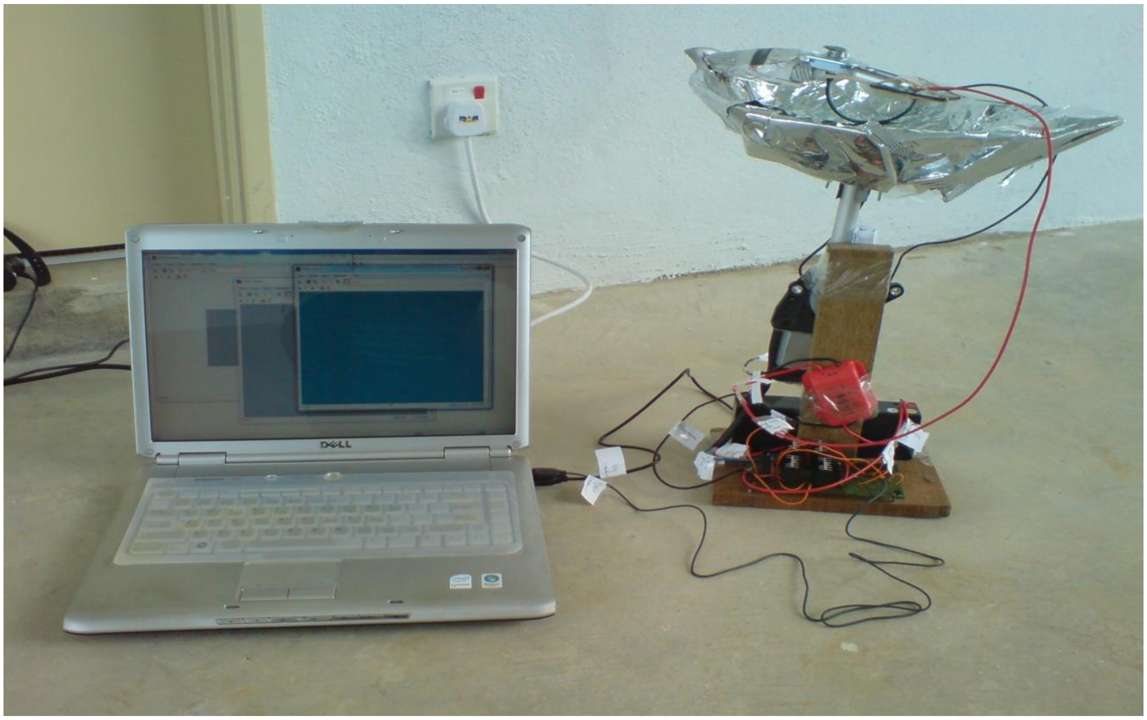

Figure 4.7: Initial Position of the System

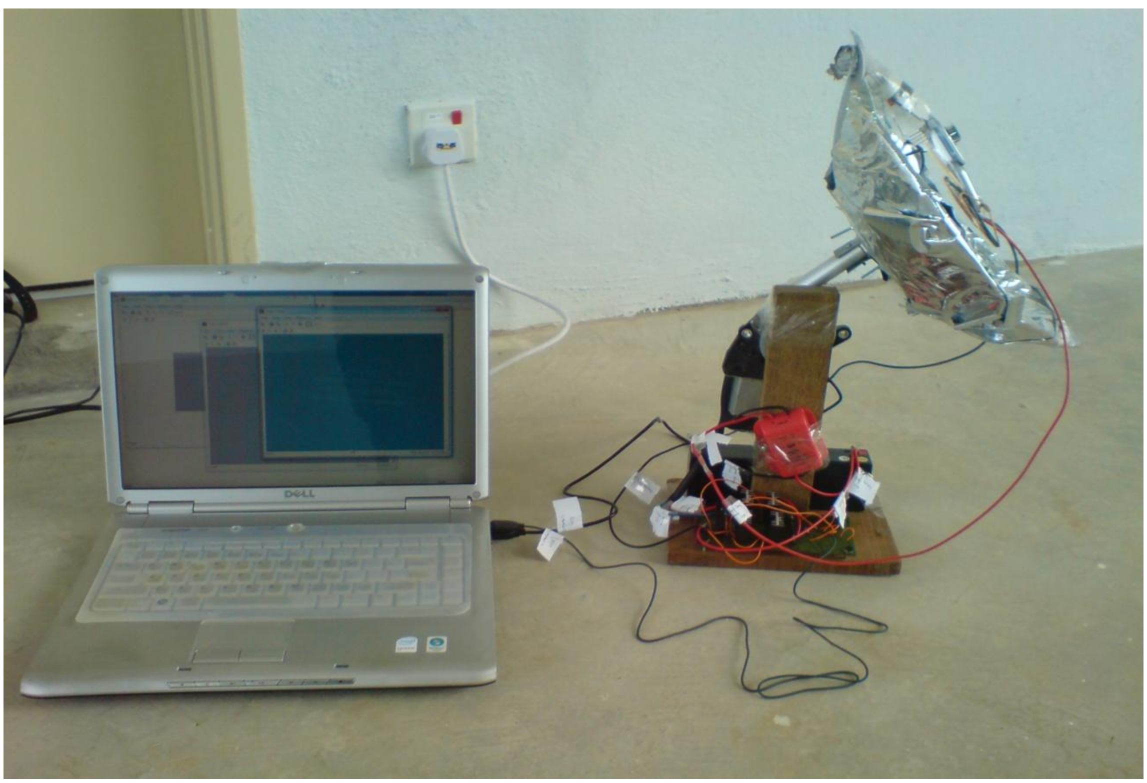

Figure 4.8: Position of System after the System Started

CHAPTER 5

CONCLUSION AND RECOMMENDATIONS

5.1 Conclusion

From the result, it is shown that one of the objectives of this project has been achieved. The flow of the system has been simulated using MATLAB/SIMULINK block set. However the main goal of the project has not yet been achieved, which is to conduct the movement of the CPC via stepper motor. This might be due to incorrect wiring concept or configuration has been made upon the circuitry for the whole system. It may also because of the solar cell power generating capability is too small and the battery running low. Thus the motor cannot get enough power to move the heavy weight of the CPC with its support.

5.2 Recommendation

It is recommended that the future development to apply for diffused reflector that is mounted around the CPC to increase the total radiation that may fall and focus onto the solar cell. At the same time, applying maximum power point tracking circuit to the solar tracking system would help much in increasing the accuracy of obtaining the maximum power. Other than that, the solar cell type is recommended to be Mono-Crystalline due to its highest power output efficiency among the rest of the solar cells.

The accuracy of the Sun Tracking System (STS) can be increase by combining the usage of MATLAB software with Programmable Intelligent Computer (PIC) programming. Utilizing PIC driving circuit will provide another choice for better controlling of the movement of the motor. As the higher the accuracy of the device, the proportion of the power received by the solar cells would be higher, resulting in the CPC will be always focusing onto the sun, regardless of the weather condition.

National Semiconductor

July 2006

LM340/LM78XX Series 3-Terminal Positive Regulators

General Description

The LM140/LM340A/LM340/LM78XXC monolithic 3-terminal positive voltage regulators employ internal current-limiting, thermal shutdown and safe-area compensation, making them essentially indestructible. If adequate heat sinking is provided, they can deliver over 1.0A output current. They are intended as fixed voltage regulators in a wide range of applications including local (on-card) regulation for elimination of noise and distribution problems associated with single-point regulation. In addition to use as fixed voltage regulators, these devices can be used with external components to obtain adjustable output voltages and currents.

Considerable effort was expended to make the entire series of regulators easy to use and minimize the number of external components. It is not necessary to bypass the output, although this does improve transient response. Input bypassing is needed only if the regulator is located far from the filter capacitor of the power supply.

The 5V, 12V, and 15V regulator options are available in the steel TO-3 power package. The LM340A/LM340/LM78XXC series is available in the TO-220 plastic power package, and the LM340-5.0 is available in the SOT-223 package, as well as the LM340-5.0 and LM340-12 in the surface-mount TO-263 package.

Features

- Complete specifications at 1A load
- Output voltage tolerances of ±2% at T_j = 25˚C and ±4% over the temperature range (LM340A)
- Line regulation of 0.01% of V_{OUT}/V of ΔV_{IN} at 1A load (LM340A)
- Load regulation of 0.3% of V_{OUT}/A (LM340A)
- Internal thermal overload protection
- Internal short-circuit current limit
- Output transistor safe area protection
- P+ Product Enhancement tested

Typical Applications

Fixed Output Regulator

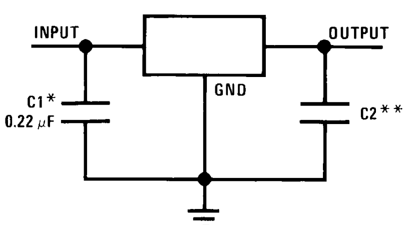

00778101

*Required if the regulator is located far from the power supply filter.

**Although no output capacitor is needed for stability, it does help transient response. (If needed, use 0.1 μF, ceramic disc).

Adjustable Output Regulator

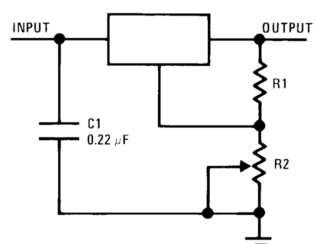

00778102

$V_{OUT} = 5V + (5V/R1 + I_Q)\ R2\ \ 5V/R1 > 3\ I_Q$,

load regulation (L_r) ≈ [(R1 + R2)/R1] (L_r of LM340-5).

Current Regulator

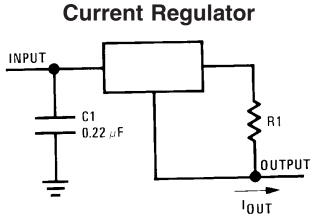

00778103

$$I_{OUT} = \frac{V2\text{-}3}{R1} + I_Q$$

ΔI_Q = 1.3 mA over line and load changes.

Comparison between SOT-223 and D-Pak (TO-252) Packages

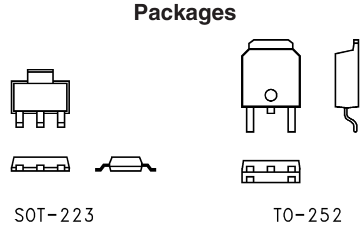

00778138

Scale 1:1

Ordering Information

Package	Temperature Range	Part Number	Packaging Marking	Transport Media	NSC Drawing
3-Lead TO-3	-55˚C to +125˚C	LM140K-5.0	LM140K 5.0P+	50 Per Tray	K02A
		LM140K-12	LM140K 12P+	50 Per Tray	
		LM140K-15	LM140K 15P+	50 Per Tray	
	0˚C to +125˚C	LM340K-5.0	LM340K 5.0 7805P+	50 Per Tray	
		LM340K-12	LM340K 12 7812P+	50 Per Tray	
		LM340K-15	LM340K 15 7815P+	50 Per Tray	
3-lead TO-220	0˚C to +125˚C	LM340AT-5.0	LM340AT 5.0 P+	45 Units/Rail	T03B
		LM340T-5.0	LM340T5 7805 P+	45 Units/Rail	
		LM340T-12	LM340T12 7812 P+	45 Units/Rail	
		LM340T-15	LM340T15 7815 P+	45 Units/Rail	
		LM7808CT	LM7808CT	45 Units/Rail	
3-Lead TO-263	0˚C to +125˚C	LM340S-5.0	LM340S-5.0 P+	45 Units/Rail	TS3B
		LM340SX-5.0		500 Units Tape and Reel	
		LM340S-12	LM340S-12 P+	45 Units/Rail	
		LM340SX-12		500 Units Tape and Reel	
		LM340AS-5.0	LM340AS-5.0 P+	45 Units/Rail	
		LM340ASX-5.0		500 Units Tape and Reel	
4-Lead SOT-223	0˚C to +125˚C	LM340MP-5.0	N00A	1k Units Tape and Reel	MP04A
		LM340MPX-5.0		2k Units Tape and Reel	
Unpackaged Die	–55˚C to 125˚C	LM140KG-5 MD8		Waffle Pack or Gel Pack	DL069089
		LM140KG-12 MD8		Waffle Pack or Gel Pack	DL059093
		LM140KG-15 MD8		Waffle Pack or Gel Pack	DL059093
	0˚C to +125˚C	LM340-5.0 MDA		Waffle Pack or Gel Pack	DI074056
		LM7808C MDC		Waffle Pack or Gel Pack	DI074056

Connection Diagrams

TO-3 Metal Can Package (K)

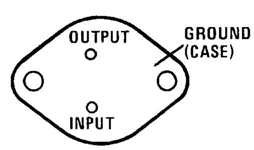

00778111

Bottom View
See Package Number K02A

TO-220 Power Package (T)

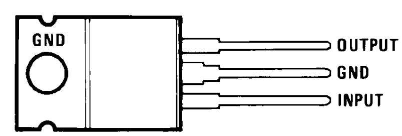

00778112

Top View
See Package Number T03B

TO-263 Surface-Mount Package (S)

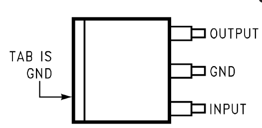

00778120

Top View
See Package Number TS3B

3-Lead SOT-223

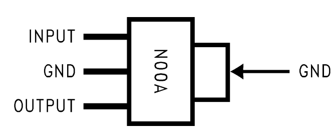

00778143

Top View
See Package Number MP04A

Absolute Maximum Ratings (Note 1)

If Military/Aerospace specified devices are required, please contact the National Semiconductor Sales Office/ Distributors for availability and specifications.

(Note 5)

DC Input Voltage	35V
Internal Power Dissipation (Note 2)	Internally Limited
Maximum Junction Temperature	150˚C
Storage Temperature Range	–65˚C to +150˚C
Lead Temperature (Soldering, 10 sec.)	
TO-3 Package (K)	300˚C
TO-220 Package (T), TO-263 Package (S)	230˚C
ESD Susceptibility (Note 3)	2 kV

Operating Conditions (Note 1)

Temperature Range (T_A) (Note 2)	
LM140	–55˚C to +125˚C
LM340A, LM340	0˚C to +125˚C
LM7808C	0˚C to +125˚C

LM340A Electrical Characteristics

I_{OUT} = 1A, 0˚C ≤ T_J ≤ + 125˚C (LM340A) unless otherwise specified (Note 4)

Symbol	Output Voltage			5V			12V			15V			Units
	Input Voltage (unless otherwise noted)			10V			19V			23V			
	Parameter	Conditions		Min	Typ	Max	Min	Typ	Max	Min	Typ	Max	
V_O	Output Voltage	T_J = 25˚C		4.9	5	5.1	11.75	12	12.25	14.7	15	15.3	V
		P_D ≤ 15W, 5 mA ≤ I_O ≤ 1A		4.8		5.2	11.5		12.5	14.4		15.6	V
		V_{MIN} ≤ V_{IN} ≤ V_{MAX}		(7.5 ≤ V_{IN} ≤ 20)			(14.8 ≤ V_{IN} ≤ 27)			(17.9 ≤ V_{IN} ≤ 30)			V
ΔV_O	Line Regulation	I_O = 500 mA				10			18			22	mV
		ΔV_{IN}		(7.5 ≤ V_{IN} ≤ 20)			(14.8 ≤ V_{IN} ≤ 27)			(17.9 ≤ V_{IN} ≤ 30)			V
		T_J = 25˚C			3	10		4	18		4	22	mV
		ΔV_{IN}		(7.5 ≤ V_{IN} ≤ 20)			(14.5 ≤ V_{IN} ≤ 27)			(17.5 ≤ V_{IN} ≤ 30)			V
		T_J = 25˚C				4			9			10	mV
		Over Temperature				12			30			30	mV
		ΔV_{IN}		(8 ≤ V_{IN} ≤ 12)			(16 ≤ V_{IN} ≤ 22)			(20 ≤ V_{IN} ≤ 26)			V
ΔV_O	Load Regulation	T_J = 25˚C	5 mA ≤ I_O ≤ 1.5A		10	25		12	32		12	35	mV
			250 mA ≤ I_O ≤ 750 mA			15			19			21	mV
		Over Temperature, 5 mA ≤ I_O ≤ 1A				25			60			75	mV
I_Q	Quiescent Current	T_J = 25˚C				6			6			6	mA
		Over Temperature				6.5			6.5			6.5	mA
ΔI_Q	Quiescent Current Change	5 mA ≤ I_O ≤ 1A			0.5			0.5			0.5		mA
		T_J = 25˚C, I_O = 1A				0.8			0.8			0.8	mA
		V_{MIN} ≤ V_{IN} ≤ V_{MAX}		(7.5 ≤ V_{IN} ≤ 20)			(14.8 ≤ V_{IN} ≤ 27)			(17.9 ≤ V_{IN} ≤ 30)			V
		I_O = 500 mA				0.8			0.8			0.8	mA
		V_{MIN} ≤ V_{IN} ≤ V_{MAX}		(8 ≤ V_{IN} ≤ 25)			(15 ≤ V_{IN} ≤ 30)			(17.9 ≤ V_{IN} ≤ 30)			V
V_N	Output Noise Voltage	T_A = 25˚C, 10 Hz ≤ f ≤ 100 kHz			40			75			90		μV
$\frac{\Delta V_{IN}}{\Delta V_{OUT}}$	Ripple Rejection	T_J = 25˚C, f = 120 Hz, I_O = 1A		68	80		61	72		60	70		dB
		or f = 120 Hz, I_O = 500 mA, Over Temperature,		68			61			60			dB
		V_{MIN} ≤ V_{IN} ≤ V_{MAX}		(8 ≤ V_{IN} ≤ 18)			(15 ≤ V_{IN} ≤ 25)			(18.5 ≤ V_{IN} ≤ 28.5)			V
R_O	Dropout Voltage	T_J = 25˚C, I_O = 1A			2.0			2.0			2.0		V
	Output Resistance	f = 1 kHz			8			18			19		mΩ
	Short-Circuit Current	T_J = 25˚C			2.1			1.5			1.2		A

LM340A Electrical Characteristics (Continued)

I_{OUT} = 1A, 0˚C ≤ T_J ≤ + 125˚C (LM340A) unless otherwise specified (Note 4)

Symbol	Output Voltage		5V			12V			15V			Units
	Input Voltage (unless otherwise noted)		10V			19V			23V			
	Parameter	Conditions	Min	Typ	Max	Min	Typ	Max	Min	Typ	Max	
	Peak Output Current	T_J = 25˚C		2.4			2.4			2.4		A
	Average TC of V_O	Min, T_J = 0˚C, I_O = 5 mA		−0.6			−1.5			−1.8		mV/˚C
V_{IN}	Input Voltage Required to Maintain Line Regulation	T_J = 25˚C	7.5			14.5			17.5			V

LM140 Electrical Characteristics (Note 4)

−55˚C ≤ T_J ≤ +150˚C unless otherwise specified

Symbol	Output Voltage			5V			12V			15V			Units
	Input Voltage (unless otherwise noted)			10V			19V			23V			
	Parameter	Conditions		Min	Typ	Max	Min	Typ	Max	Min	Typ	Max	
V_O	Output Voltage	T_J = 25˚C, 5 mA ≤ I_O ≤ 1A		4.8	5	5.2	11.5	12	12.5	14.4	15	15.6	V
		P_D ≤ 15W, 5 mA ≤ I_O ≤ 1A		4.75		5.25	11.4		12.6	14.25		15.75	V
		V_{MIN} ≤ V_{IN} ≤ V_{MAX}			(8 ≤ V_{IN} ≤ 20)			(15.5 ≤ V_{IN} ≤ 27)			(18.5 ≤ V_{IN} ≤ 30)		V
ΔV_O	Line Regulation	I_O = 500 mA	T_J = 25˚C		3	50		4	120		4	150	mV
			ΔV_{IN}		(7 ≤ V_{IN} ≤ 25)			(14.5 ≤ V_{IN} ≤ 30)			(17.5 ≤ V_{IN} ≤ 30)		V
			−55˚C ≤ T_J ≤ +150˚C			50			120			150	mV
			ΔV_{IN}		(8 ≤ V_{IN} ≤ 20)			(15 ≤ V_{IN} ≤ 27)			(18.5 ≤ V_{IN} ≤ 30)		V
		I_O ≤ 1A	T_J = 25˚C			50			120			150	mV
			ΔV_{IN}		(7.5 ≤ V_{IN} ≤ 20)			(14.6 ≤ V_{IN} ≤ 27)			(17.7 ≤ V_{IN} ≤ 30)		V
			−55˚C ≤ T_J ≤ +150˚C			25			60			75	mV
			ΔV_{IN}		(8 ≤ V_{IN} ≤ 12)			(16 ≤ V_{IN} ≤ 22)			(20 ≤ V_{IN} ≤ 26)		V
ΔV_O	Load Regulation	T_J = 25˚C	5 mA ≤ I_O ≤ 1.5A		10	50		12	120		12	150	mV
			250 mA ≤ I_P ≤ 750 mA			25			60			75	mV
		−55˚C ≤ T_J ≤ +150˚C, 5 mA ≤ I_O ≤ 1A				50			120			150	mV
I_Q	Quiescent Current	I_O ≤ 1A	T_J = 25˚C			6			6			6	mA
			−55˚C ≤ T_J ≤ +150˚C			7			7			7	mA
ΔI_Q	Quiescent Current Change	5 mA ≤ I_O ≤ 1A			0.5			0.5			0.5		mA
		T_J = 25˚C, I_O ≤ 1A				0.8			0.8			0.8	mA
		V_{MIN} ≤ V_{IN} ≤ V_{MAX}			(8 ≤ V_{IN} ≤ 20)			(15 ≤ V_{IN} ≤ 27)			(18.5 ≤ V_{IN} ≤ 30)		V
		I_O = 500 mA, −55˚C ≤ T_J ≤ +150˚C				0.8			0.8			0.8	mA
		V_{MIN} ≤ V_{IN} ≤ V_{MAX}			(8 ≤ V_{IN} ≤ 25)			(15 ≤ V_{IN} ≤ 30)			(18.5 ≤ V_{IN} ≤ 30)		V
V_N	Output Noise Voltage	T_A = 25˚C, 10 Hz ≤ f ≤ 100 kHz			40			75			90		μV

LM140 Electrical Characteristics (Note 4) (Continued)

$-55^\circ C \le T_J \le +150^\circ C$ unless otherwise specified

Symbol	Output Voltage			5V			12V			15V			Units
	Input Voltage (unless otherwise noted)			10V			19V			23V			
	Parameter	Conditions		Min	Typ	Max	Min	Typ	Max	Min	Typ	Max	
$\frac{\Delta V_{IN}}{\Delta V_{OUT}}$	Ripple Rejection	f = 120 Hz	$I_O \le 1A$, $T_J = 25^\circ C$ or	68	80		61	72		60	70		dB
			$I_O \le 500$ mA, $-55^\circ C \le T_J \le +150^\circ C$	68			61			60			dB
		$V_{MIN} \le V_{IN} \le V_{MAX}$		$(8 \le V_{IN} \le 18)$			$(15 \le V_{IN} \le 25)$			$(18.5 \le V_{IN} \le 28.5)$			V
R_O	Dropout Voltage	$T_J = 25^\circ C$, $I_O = 1A$			2.0			2.0			2.0		V
	Output Resistance	f = 1 kHz			8			18			19		mΩ
	Short-Circuit Current	$T_J = 25^\circ C$			2.1			1.5			1.2		A
	Peak Output Current	$T_J = 25^\circ C$			2.4			2.4			2.4		A
	Average TC of V_{OUT}	$0^\circ C \le T_J \le +150^\circ C$, $I_O = 5$ mA			−0.6			−1.5			−1.8		mV/°C
V_{IN}	Input Voltage Required to Maintain Line Regulation	$T_J = 25^\circ C$, $I_O \le 1A$		7.5			14.6			17.7			V

LM340 Electrical Characteristics (Note 4)

$0^\circ C \le T_J \le +125^\circ C$ unless otherwise specified

Symbol	Output Voltage			5V			12V			15V			Units
	Input Voltage (unless otherwise noted)			10V			19V			23V			
	Parameter	Conditions		Min	Typ	Max	Min	Typ	Max	Min	Typ	Max	
V_O	Output Voltage	$T_J = 25^\circ C$, 5 mA $\le I_O \le 1A$		4.8	5	5.2	11.5	12	12.5	14.4	15	15.6	V
		$P_D \le 15W$, 5 mA $\le I_O \le 1A$		4.75		5.25	11.4		12.6	14.25		15.75	V
		$V_{MIN} \le V_{IN} \le V_{MAX}$		$(7.5 \le V_{IN} \le 20)$			$(14.5 \le V_{IN} \le 27)$			$(17.5 \le V_{IN} \le 30)$			V
ΔV_O	Line Regulation	$I_O = 500$ mA	$T_J = 25^\circ C$		3	50		4	120		4	150	mV
			ΔV_{IN}	$(7 \le V_{IN} \le 25)$			$(14.5 \le V_{IN} \le 30)$			$(17.5 \le V_{IN} \le 30)$			V
			$0^\circ C \le T_J \le +125^\circ C$			50			120			150	mV
			ΔV_{IN}	$(8 \le V_{IN} \le 20)$			$(15 \le V_{IN} \le 27)$			$(18.5 \le V_{IN} \le 30)$			V
		$I_O \le 1A$	$T_J = 25^\circ C$			50			120			150	mV
			ΔV_{IN}	$(7.5 \le V_{IN} \le 20)$			$(14.6 \le V_{IN} \le 27)$			$(17.7 \le V_{IN} \le 30)$			V
			$0^\circ C \le T_J \le +125^\circ C$			25			60			75	mV
			ΔV_{IN}	$(8 \le V_{IN} \le 12)$			$(16 \le V_{IN} \le 22)$			$(20 \le V_{IN} \le 26)$			V
ΔV_O	Load Regulation	$T_J = 25^\circ C$	5 mA $\le I_O \le 1.5A$		10	50		12	120		12	150	mV
			250 mA $\le I_O \le 750$ mA			25			60			75	mV
		5 mA $\le I_O \le 1A$, $0^\circ C \le T_J \le +125^\circ C$				50			120			150	mV
I_Q	Quiescent Current	$I_O \le 1A$	$T_J = 25^\circ C$			8			8			8	mA
			$0^\circ C \le T_J \le +125^\circ C$			8.5			8.5			8.5	mA
ΔI_Q	Quiescent Current Change	5 mA $\le I_O \le 1A$			0.5			0.5			0.5		mA
		$T_J = 25^\circ C$, $I_O \le 1A$				1.0			1.0			1.0	mA

LM340 Electrical Characteristics (Note 4) (Continued)

$0^{\circ}C \le T_J \le +125^{\circ}C$ unless otherwise specified

Symbol	Output Voltage		5V			12V			15V			Units
	Input Voltage (unless otherwise noted)		10V			19V			23V			
	Parameter	Conditions	Min	Typ	Max	Min	Typ	Max	Min	Typ	Max	
		$V_{MIN} \le V_{IN} \le V_{MAX}$		$(7.5 \le V_{IN} \le 20)$			$(14.8 \le V_{IN} \le 27)$			$(17.9 \le V_{IN} \le 30)$		V
		$I_O \le 500$ mA, $0^{\circ}C \le T_J \le +125^{\circ}C$			1.0			1.0			1.0	mA
		$V_{MIN} \le V_{IN} \le V_{MAX}$		$(7 \le V_{IN} \le 25)$			$(14.5 \le V_{IN} \le 30)$			$(17.5 \le V_{IN} \le 30)$		V
V_N	Output Noise Voltage	$T_A = 25^{\circ}C$, 10 Hz $\le f \le$ 100 kHz		40			75			90		µV
$\frac{\Delta V_{IN}}{\Delta V_{OUT}}$	Ripple Rejection	f = 120 Hz, $I_O \le 1A$, $T_J = 25^{\circ}C$	62	80		55	72		54	70		dB
		f = 120 Hz, or $I_O \le 500$ mA, $0^{\circ}C \le T_J \le +125^{\circ}C$	62			55			54			dB
		$V_{MIN} \le V_{IN} \le V_{MAX}$		$(8 \le V_{IN} \le 18)$			$(15 \le V_{IN} \le 25)$			$(18.5 \le V_{IN} \le 28.5)$		V
R_O	Dropout Voltage	$T_J = 25^{\circ}C$, $I_O = 1A$		2.0			2.0			2.0		V
	Output Resistance	f = 1 kHz		8			18			19		mΩ
	Short-Circuit Current	$T_J = 25^{\circ}C$		2.1			1.5			1.2		A
	Peak Output Current	$T_J = 25^{\circ}C$		2.4			2.4			2.4		A
	Average TC of V_{OUT}	$0^{\circ}C \le T_J \le +125^{\circ}C$, $I_O = 5$ mA		–0.6			–1.5			–1.8		mV/°C
V_{IN}	Input Voltage Required to Maintain Line Regulation	$T_J = 25^{\circ}C$, $I_O \le 1A$	7.5			14.6			17.7			V

Note 1: Absolute Maximum Ratings are limits beyond which damage to the device may occur. Operating Conditions are conditions under which the device functions but the specifications might not be guaranteed. For guaranteed specifications and test conditions see the Electrical Characteristics.

Note 2: The maximum allowable power dissipation at any ambient temperature is a function of the maximum junction temperature for operation ($T_{JMAX} = 125^{\circ}C$ or $150^{\circ}C$), the junction-to-ambient thermal resistance (θ_{JA}), and the ambient temperature (T_A). $P_{DMAX} = (T_{JMAX} - T_A)/\theta_{JA}$. If this dissipation is exceeded, the die temperature will rise above T_{JMAX} and the electrical specifications do not apply. If the die temperature rises above 150°C, the device will go into thermal shutdown. For the TO-3 package (K, KC), the junction-to-ambient thermal resistance (θ_{JA}) is 39°C/W. When using a heatsink, θ_{JA} is the sum of the 4°C/W junction-to-case thermal resistance (θ_{JC}) of the TO-3 package and the case-to-ambient thermal resistance of the heatsink. For the TO-220 package (T), θ_{JA} is 54°C/W and θ_{JC} is 4°C/W. If SOT-223 is used, the junction-to-ambient thermal resistance is 174°C/W and can be reduced by a heatsink (see Applications Hints on heatsinking).

If the TO-263 package is used, the thermal resistance can be reduced by increasing the PC board copper area thermally connected to the package: Using 0.5 square inches of copper area, θ_{JA} is 50°C/W; with 1 square inch of copper area, $\theta_{JA}$is 37°C/W; and with 1.6 or more inches of copper area, θ_{JA} is 32°C/W.

Note 3: ESD rating is based on the human body model, 100 pF discharged through 1.5 kΩ.

Note 4: All characteristics are measured with a 0.22 µF capacitor from input to ground and a 0.1 µF capacitor from output to ground. All characteristics except noise voltage and ripple rejection ratio are measured using pulse techniques ($t_w \le 10$ ms, duty cycle $\le 5\%$). Output voltage changes due to changes in internal temperature must be taken into account separately.

Note 5: Military datasheets are available upon request. At the time of printing, the military datasheet specifications for the LM140K-5.0/883, LM140K-12/883, and LM140K-15/883 complied with the min and max limits for the respective versions of the LM140. The LM140H and LM140K may also be procured as JAN devices on slash sheet JM38510/107.

LM7808C
Electrical Characteristics

$0^\circ C \leq T_J \leq +150^\circ C$, $V_I = 14V$, $I_O = 500$ mA, $C_I = 0.33$ μF, $C_O = 0.1$ μF, unless otherwise specified

Symbol	Parameter		Conditions (Note 6)		LM7808C Min	LM7808C Typ	LM7808C Max	Units
V_O	Output Voltage		$T_J = 25^\circ C$		7.7	8.0	8.3	V
ΔV_O	Line Regulation		$T_J = 25^\circ C$	$10.5V \leq V_I \leq 25V$		6.0	160	mV
				$11.0V \leq V_I \leq 17V$		2.0	80	
ΔV_O	Load Regulation		$T_J = 25^\circ C$	$5.0\text{ mA} \leq I_O \leq 1.5A$		12	160	mV
				$250\text{ mA} \leq I_O \leq 750$ mA		4.0	80	
V_O	Output Voltage		$11.5V \leq V_I \leq 23V$, $5.0\text{ mA} \leq I_O \leq 1.0A$, $P \leq 15W$		7.6		8.4	V
I_Q	Quiescent Current		$T_J = 25^\circ C$			4.3	8.0	mA
ΔI_Q	Quiescent Current Change	With Line	$11.5V \leq V_I \leq 25V$				1.0	mA
		With Load	$5.0\text{ mA} \leq I_O \leq 1.0A$				0.5	
V_N	Noise		$T_A = 25^\circ C$, $10\text{ Hz} \leq f \leq 100$ kHz			52		μV
$\Delta V_I/\Delta V_O$	Ripple Rejection		$f = 120$ Hz, $I_O = 350$ mA, $T_J = 25^\circ C$		56	72		dB
V_{DO}	Dropout Voltage		$I_O = 1.0A$, $T_J = 25^\circ C$			2.0		V
R_O	Output Resistance		$f = 1.0$ kHz			16		mΩ
I_{OS}	Output Short Circuit Current		$T_J = 25^\circ C$, $V_I = 35V$			0.45		A
I_{PK}	Peak Output Current		$T_J = 25^\circ C$			2.2		A
$\Delta V_O/\Delta T$	Average Temperature Coefficient of Output Voltage		$I_O = 5.0$ mA			0.8		mV/°C

Note 6: All characteristics are measured with a 0.22 μF capacitor from input to ground and a 0.1 μF capacitor from output to ground. All characteristics except noise voltage and ripple rejection ratio are measured using pulse techniques ($t_w \leq 10$ ms, duty cycle ≤ 5%). Output voltage changes due to changes in internal temperature must be taken into account separately.

Typical Performance Characteristics

Maximum Average Power Dissipation

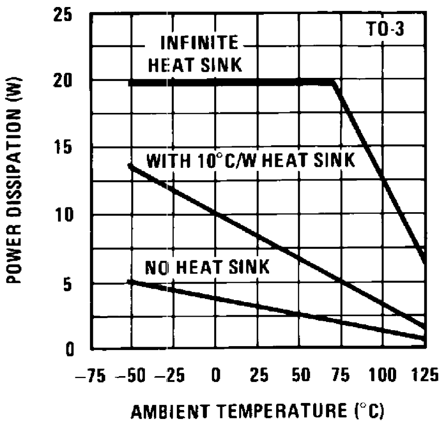

00778122

Maximum Average Power Dissipation

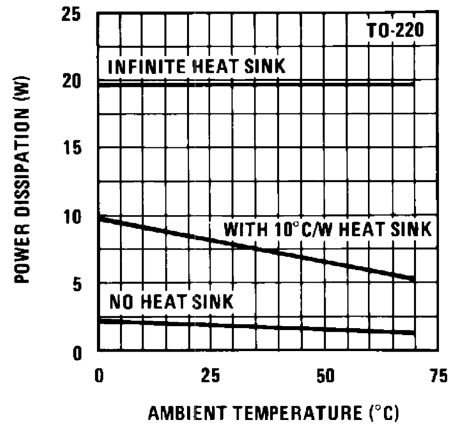

00778123

Maximum Power Dissipation (TO-263) (See Note 2)

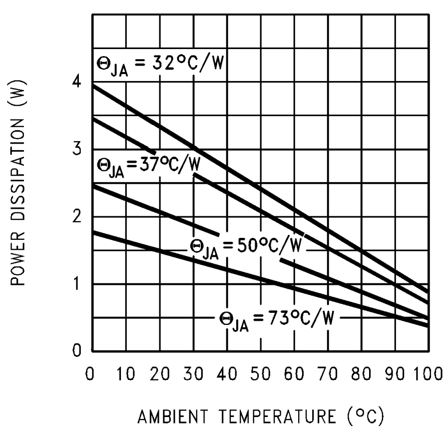

00778124

Output Voltage (Normalized to 1V at T_J = 25°C)

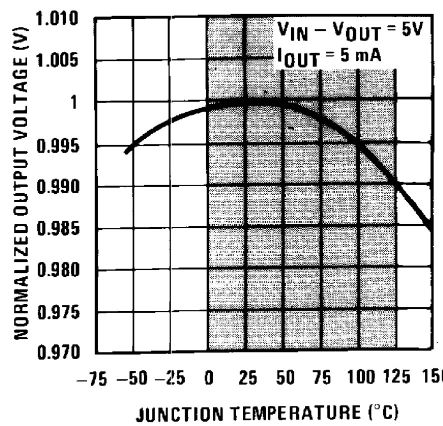

00778125

Note: Shaded area refers to LM340A/LM340, LM7805C, LM7812C and LM7815C.

Ripple Rejection

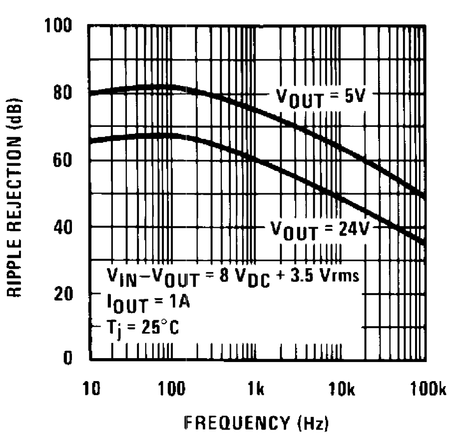

00778126

Ripple Rejection

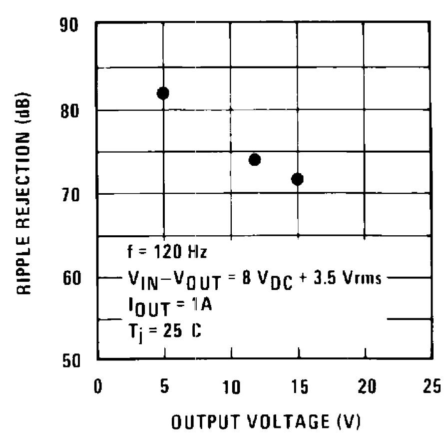

00778127

Typical Performance Characteristics (Continued)

Output Impedance

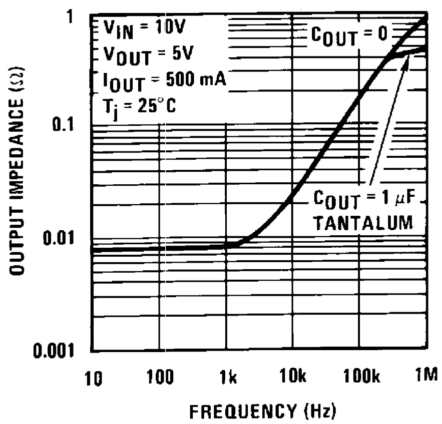

00778128

Dropout Characteristics

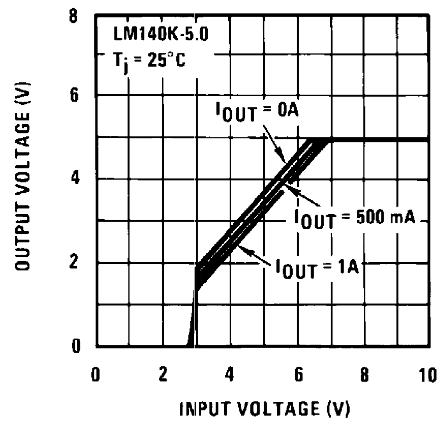

00778129

Quiescent Current

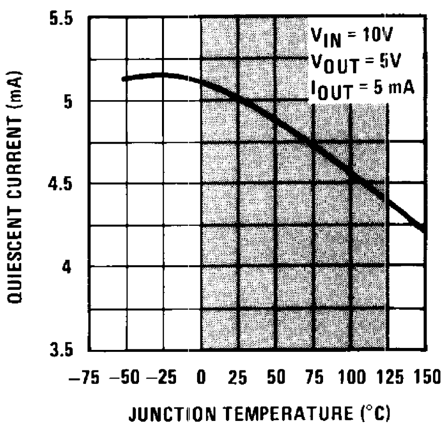

00778130

Note: Shaded area refers to LM340A/LM340, LM7805C, LM7812C and LM7815C.

Peak Output Current

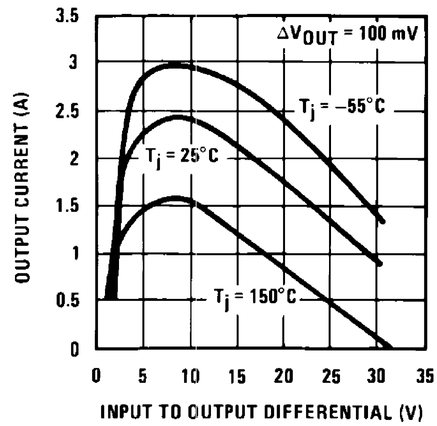

00778131

Dropout Voltage

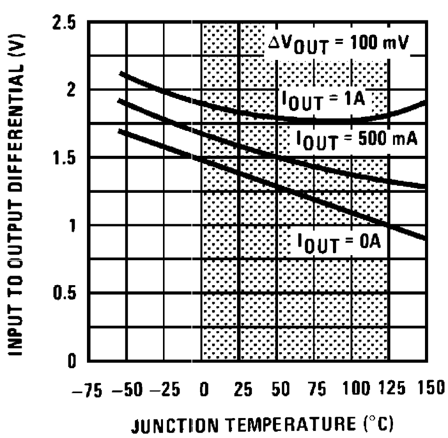

00778132

Note: Shaded area refers to LM340A/LM340, LM7805C, LM7812C and LM7815C.

Quiescent Current

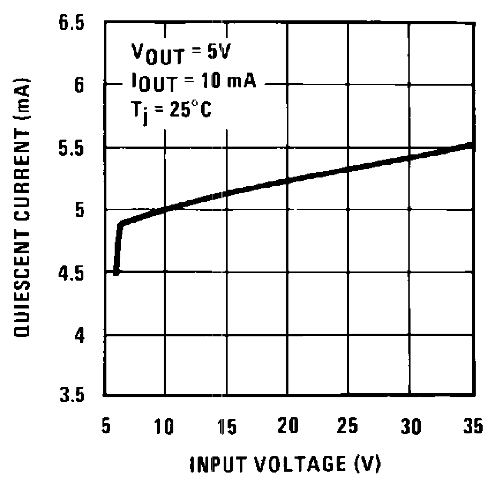

00778133

Line Regulation
140AK-5.0, I_{OUT} = 1A, T_A = 25˚C

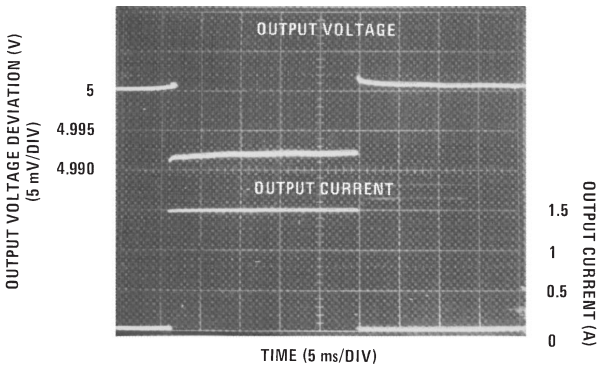

00778105

Line Regulation
140AK-5.0, V_{IN} = 10V, T_A = 25˚C

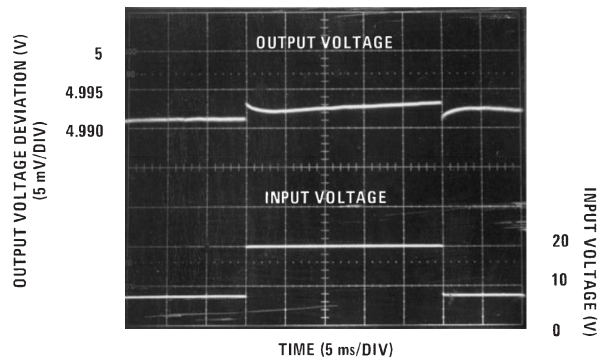

00778106

Equivalent Schematic

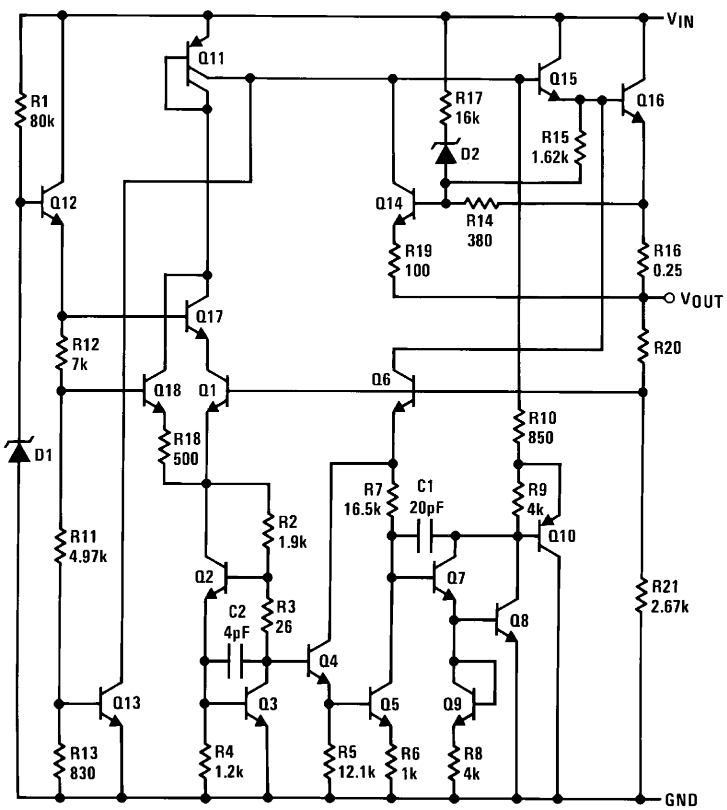

00778107

Application Hints

The LM340/LM78XX series is designed with thermal protection, output short-circuit protection and output transistor safe area protection. However, as with *any* IC regulator, it becomes necessary to take precautions to assure that the regulator is not inadvertently damaged. The following describes possible misapplications and methods to prevent damage to the regulator.

SHORTING THE REGULATOR INPUT

When using large capacitors at the output of these regulators, a protection diode connected input to output (*Figure 1*) may be required if the input is shorted to ground. Without the protection diode, an input short will cause the input to rapidly approach ground potential, while the output remains near the initial V_{OUT}because of the stored charge in the large output capacitor. The capacitor will then discharge through a large internal input to output diode and parasitic transistors. If the energy released by the capacitor is large enough, this diode, low current metal and the regulator will be destroyed. The fast diode in *Figure 1* will shunt most of the capacitors discharge current around the regulator. Generally no protection diode is required for values of output capacitance ≤ 10 µF.

RAISING THE OUTPUT VOLTAGE ABOVE THE INPUT VOLTAGE

Since the output of the device does not sink current, forcing the output high can cause damage to internal low current paths in a manner similar to that just described in the "Shorting the Regulator Input" section.

REGULATOR FLOATING GROUND (*Figure 2*)

When the ground pin alone becomes disconnected, the output approaches the unregulated input, causing possible damage to other circuits connected to V_{OUT}. If ground is reconnected with power "ON", damage may also occur to the regulator. This fault is most likely to occur when plugging in regulators or modules with on card regulators into powered up sockets. Power should be turned off first, thermal limit ceases operating, or ground should be connected first if power must be left on.

TRANSIENT VOLTAGES

If transients exceed the maximum rated input voltage of the device, or reach more than 0.8V below ground and have sufficient energy, they will damage the regulator. The solution is to use a large input capacitor, a series input breakdown diode, a choke, a transient suppressor or a combination of these.

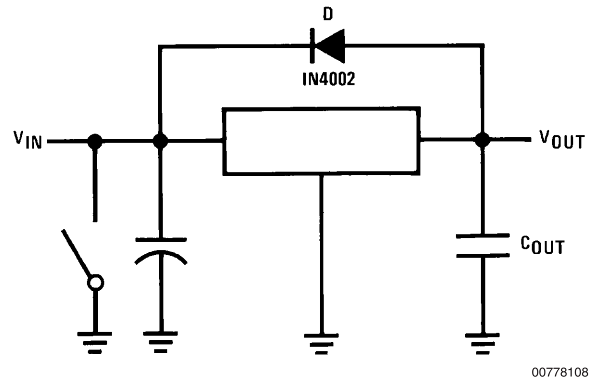

FIGURE 1. Input Short

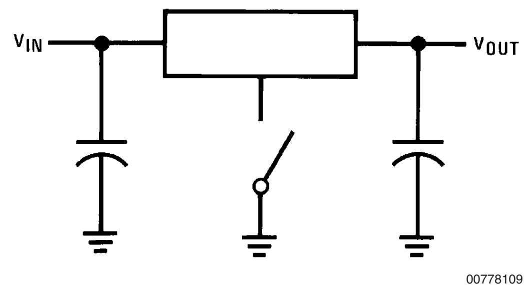

FIGURE 2. Regulator Floating Ground

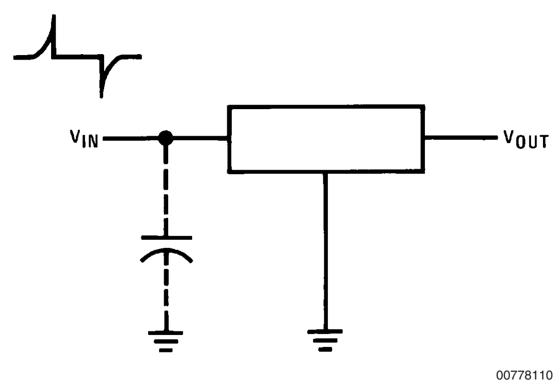

FIGURE 3. Transients

When a value for $\theta_{(H-A)}$ is found using the equation shown, a heatsink must be selected that has *a value that is less than or equal to this number.*

$\theta_{(H-A)}$ is specified numerically by the heatsink manufacturer in this catalog, or shown in a curve that plots temperature rise vs power dissipation for the heatsink.

Application Hints (Continued)

HEATSINKING TO-263 AND SOT-223 PACKAGE PARTS

Both the TO-263 (“S”) and SOT-223 (“MP”) packages use a copper plane on the PCB and the PCB itself as a heatsink. To optimize the heat sinking ability of the plane and PCB, solder the tab of the plane.

shows for the TO-263 the measured values of $\theta_{(J-A)}$ for different copper area sizes using a typical PCB with 1 ounce copper *and no solder mask over the copper area used for heatsinking*.

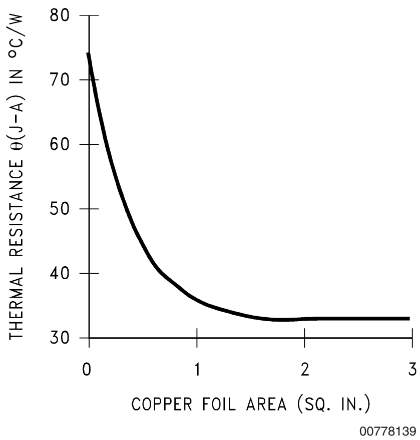

FIGURE 4. $\theta_{(J-A)}$ vs Copper (1 ounce) Area for the TO-263 Package

As shown in the figure, increasing the copper area beyond 1 square inch produces very little improvement. It should also be observed that the minimum value of $\theta_{(J-A)}$ for the TO-263 package mounted to a PCB is 32˚C/W.

As a design aid, *Figure 5* shows the maximum allowable power dissipation compared to ambient temperature for the TO-263 device (assuming $\theta_{(J-A)}$ is 35˚C/W and the maximum junction temperature is 125˚C).

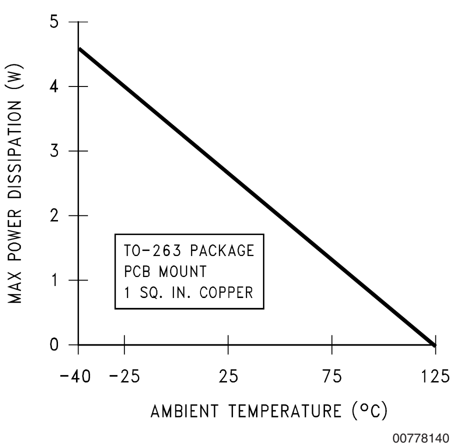

FIGURE 5. Maximum Power Dissipation vs T_{AMB} for the TO-263 Package

Figures 6, 7 show the information for the SOT-223 package. *Figure 6* assumes a $\theta_{(J-A)}$ of 74˚C/W for 1 ounce copper and 51˚C/W for 2 ounce copper and a maximum junction temperature of 125˚C.

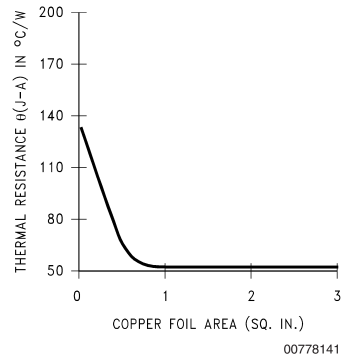

FIGURE 6. $\theta_{(J-A)}$ vs Copper (2 ounce) Area for the SOT-223 Package

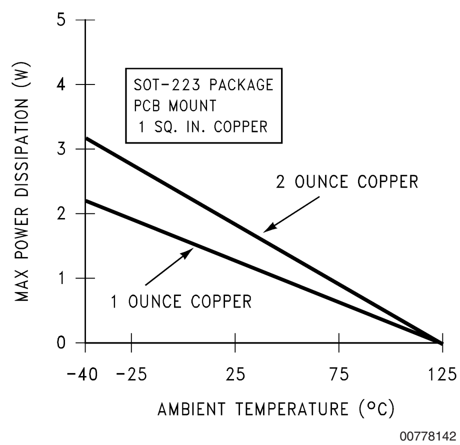

FIGURE 7. Maximum Power Dissipation vs T_{AMB} for the SOT-223 Package

Please see AN-1028 for power enhancement techniques to be used with the SOT-223 package.

Typical Applications

Fixed Output Regulator

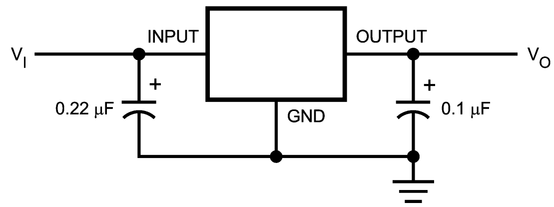

00778113

Note: Bypass capacitors are recommended for optimum stability and transient response, and should be located as close as possible to the regulator.

High Input Voltage Circuits

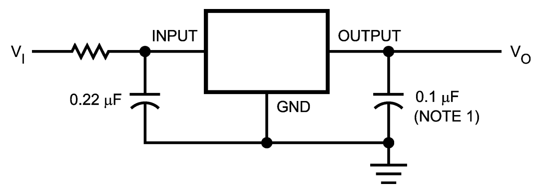

00778114

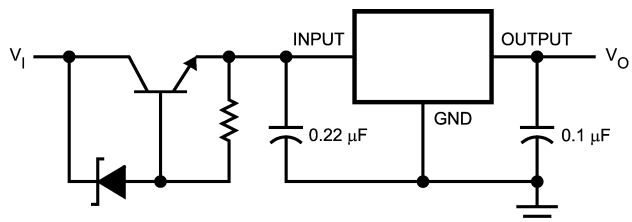

00778115

High Current Voltage Regulator

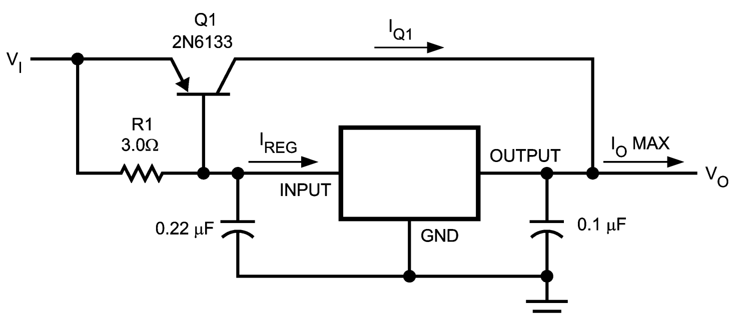

00778116

$$\beta(Q1) \geq \frac{I_{O\,Max}}{I_{REG\,Max}}$$

$$R1 = \frac{0.9}{I_{REG}} = \frac{\beta(Q1)\,V_{BE(Q1)}}{I_{REG\,Max}\,(\beta + 1) - I_{O\,Max}}$$

Typical Applications (Continued)

High Output Current, Short Circuit Protected

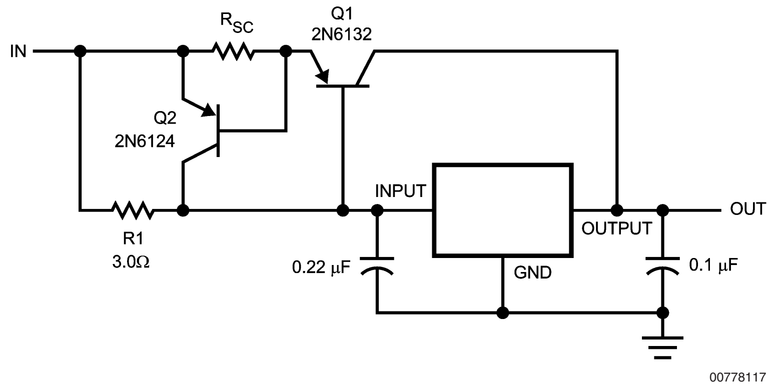

$$R_{SC} = \frac{0.8}{I_{SC}}$$

$$R1 = \frac{\beta V_{BE(Q1)}}{I_{REG\ Max}(\beta + 1) - I_{O\ Max}}$$

Positive and Negative Regulator

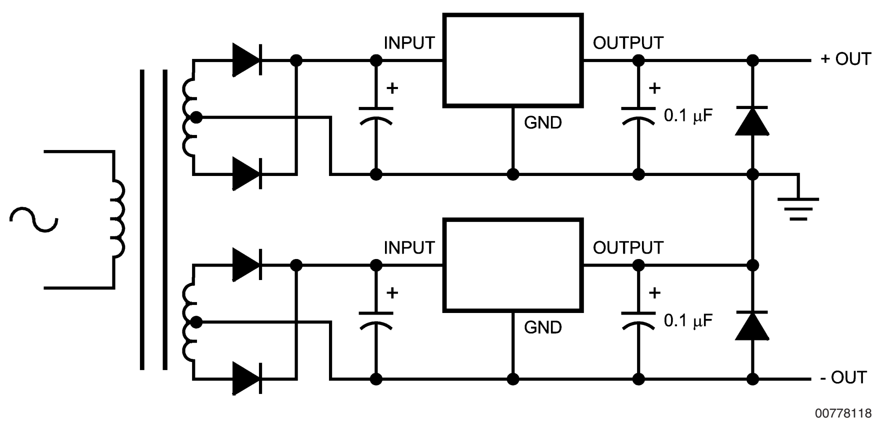

Physical Dimensions inches (millimeters) unless otherwise noted

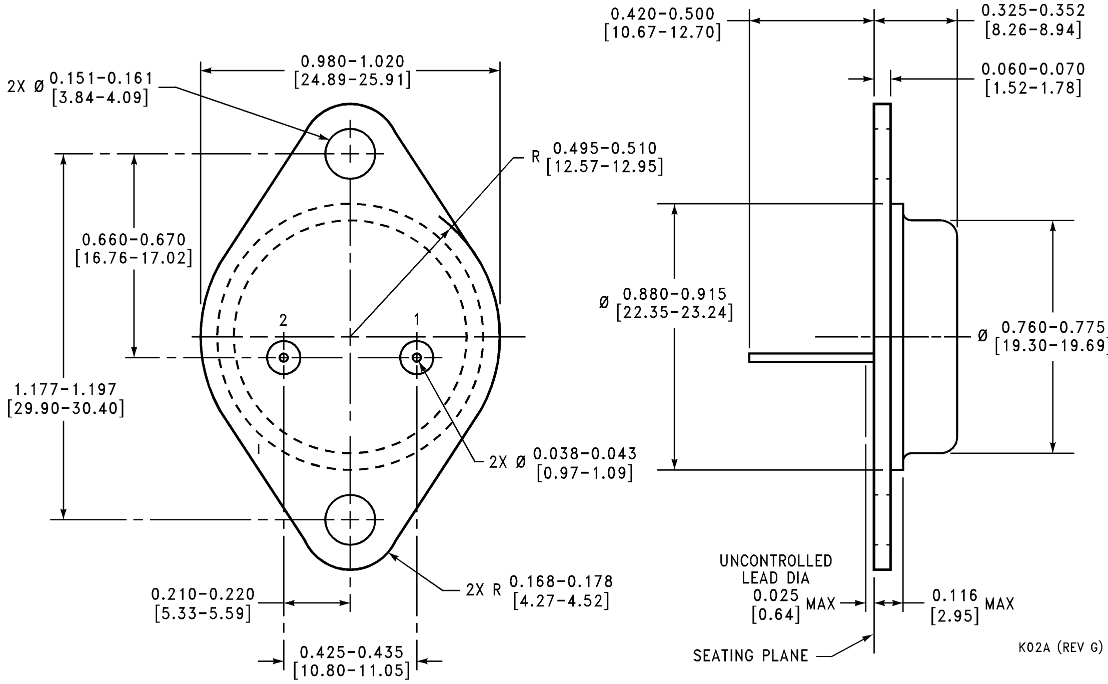

TO-3 Metal Can Package (K)
NS Package Number K02A

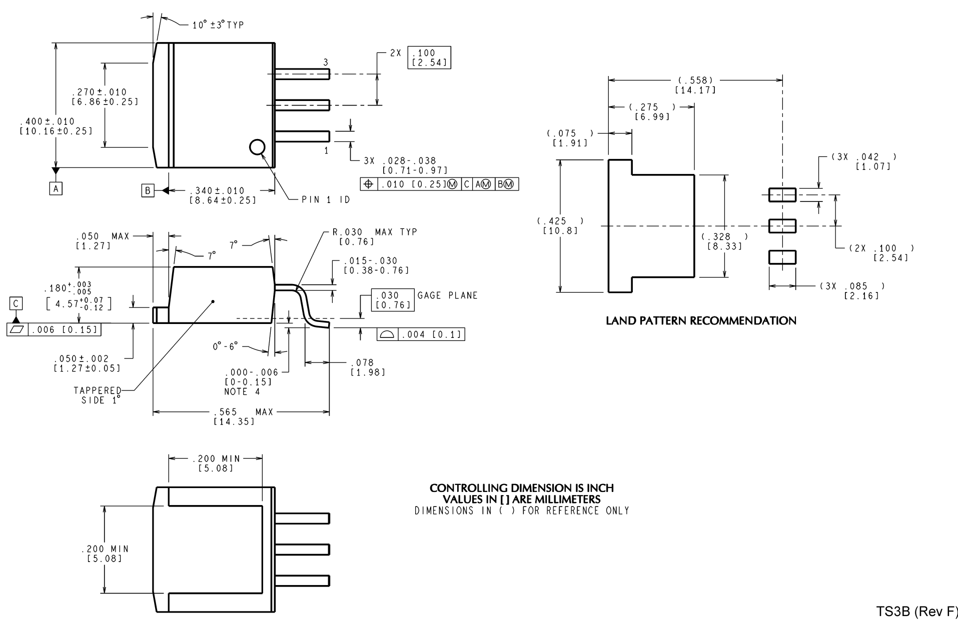

TO-263 Surface-Mount Package (S)
NS Package Number TS3B

Physical Dimensions inches (millimeters) unless otherwise noted (Continued)

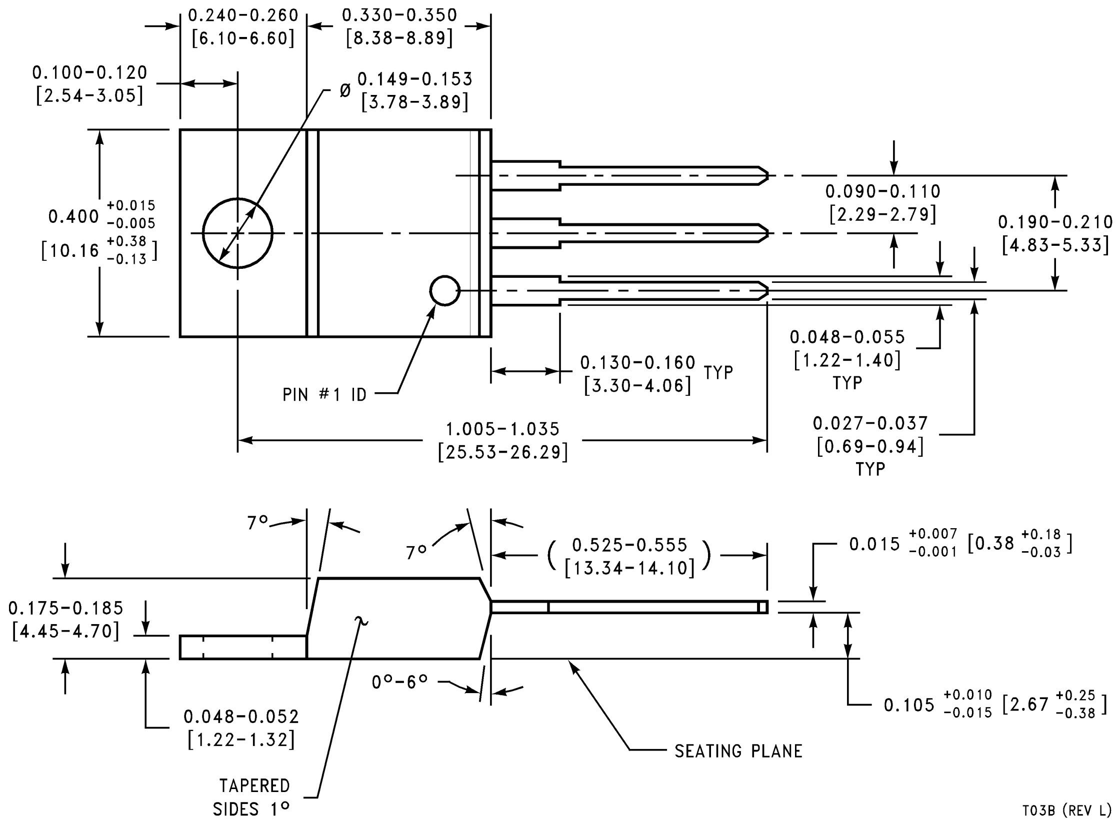

TO-220 Power Package (T)
NS Package Number T03B

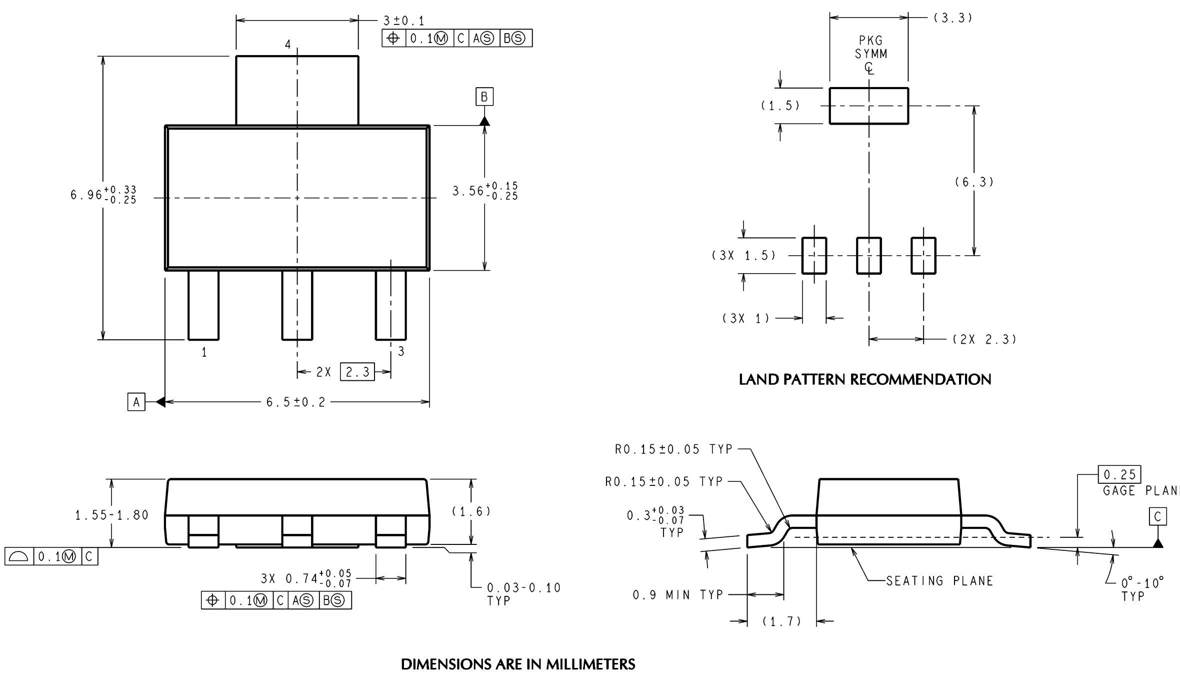

MP04A (Rev B)

3-Lead SOT-223 Package
NS Package Number MP04A

Notes

National Semiconductor
Americas Customer
Support Center
Email: new.feedback@nsc.com
Tel: 1-800-272-9959

www.national.com

National Semiconductor
Europe Customer Support Center
Fax: +49 (0) 180-530 85 86
Email: europe.support@nsc.com
Deutsch Tel: +49 (0) 69 9508 6208
English Tel: +44 (0) 870 24 0 2171
Français Tel: +33 (0) 1 41 91 8790

National Semiconductor
Asia Pacific Customer
Support Center
Email: ap.support@nsc.com

National Semiconductor
Japan Customer Support Center
Fax: 81-3-5639-7507
Email: jpn.feedback@nsc.com
Tel: 81-3-5639-7560

IRF530/531/532/533
IRFP130/131/132/133

N-CHANNEL POWER MOSFETS

FEATURES

- Lower $R_{DS\ (ON)}$
- Improved inductive ruggedness
- Fast switching times
- Rugged polysilicon gate cell structure
- Lower input capacitance
- Extended safe operating area
- Improved high temperature reliability

TO-220

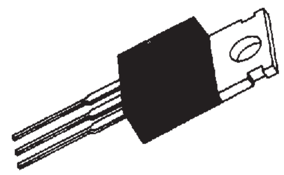

IRF530/531/532/533

TO-3P

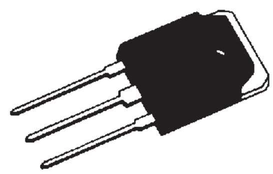

IRFP130/131/132/133

PRODUCT SUMMARY

Part Number	V_{DS}	$R_{DS(on)}$	I_D
IRF530/IRFP130	100V	0.16Ω	14A
IRF531/IRFP131	80V	0.16Ω	14A
IRF532/IRFP132	100V	0.23Ω	12A
IRF533/IRFP133	80V	0.23Ω	12A

MAXIMUM RATINGS

Characteristics	Symbol	IRF530 IRFP130	IRF531 IRFP131	IRF532 IRFP132	IRF533 IRFP133	Unit
Drain-Source Voltage (1)	V_{DSS}	100	80	100	80	Vdc
Drain-Gate Voltage (R_{GS}=1.0MΩ)(1)	V_{DGR}	100	80	100	80	Vdc
Gate-Source Voltage	V_{GS}	±20				Vdc
Continuous Drain Current T_C=25°C	I_D	14	14	12	12	Adc
Continuous Drain Current T_C=100°C	I_D	10	10	8.3	8.3	Adc
Drain Current—Pulsed (3)	I_{DM}	56	56	48	48	Adc
Gate Current—Pulsed	I_{GM}	±1.5				Adc
Single Pulsed Avalanche Energy (4)	E_{AS}	69				mJ
Avalanche Current	I_{AS}	14				A
Total Power Dissipation @ T_C=25°C Derate above 25°C	P_D	77 0.62				Watts W/°C
Operating and Storage Junction to Case	T_J, Tstg	−55 to 150				°C
Maximum Lead Temp. for Soldering Purposes, 1/8″ from case for 5 seconds	T_L	300				°C

Notes: (1) T_J=25°C to 150°C
(2) Pulse test: Pulse width≤300μs, Duty Cycle≤2%
(3) Repetitive rating: Pulse with limited by max. junction temperature
(4) L=0.53 mH, V_{dd}=25V, R_G=25Ω, Starting T_j=25°C

IRF530/531/532/533
IRFP130/131/132/133

N-CHANNEL POWER MOSFETS

ELECTRICAL CHARACTERISTICS (T_C=25°C unless otherwise specified)

Symbol	Characteristic	Min	Typ	Max	Units	Test Conditions
BV_{DSS}	Drain-Source Breakdown Voltage IRF530/IRFP130 IRF532/IRFP132	100	—	—	V	V_{GS}=0V I_D=250μA
	IRF531/IRFP131 IRF533/IRFP133	80	—	—	V	
$V_{GS(th)}$	Gate Threshold Voltage	2.0	—	4.0	V	$V_{DS}=V_{GS}$, I_D=250μA
I_{GSS}	Gate-Source Leakage Forward	—	—	100	nA	V_{GS}=20V
I_{GSS}	Gate-Source Leakage Reverse	—	—	−100	nA	V_{GS}=−20V
I_{DSS}	Zero Gate Voltage Drain Current	—	—	250	μA	V_{DS}=Max. Rating, V_{GS}=0V
		—	—	1000	μA	V_{DS}=Max. Rating×0 8, V_{GS}=0V, T_C=125°C
$I_{D(on)}$	On-State Drain-Source Current (2) IRF530/IRFP130 IRF531/IRFP131	14	—	—	A	V_{DS}≥3.2V, V_{GS}=10V
	IRF532/IRFP132 IRF533/IRFP133	12	—	—	A	
$R_{DS(on)}$	Static Drain-Source On-State Resistance (2) IRF530/IRFP130 IRF531/IRFP131	—	0.10	0.16	Ω	V_{GS}=10V, I_D=8.3A
	IRF532/IRFP132 IRF533/IRFP133	—	0.16	0.23	Ω	
g_{fs}	Forward Transconductance (2)	5.1	7.6	—	℧	V_{DS}≥50V, I_D=8.3A
C_{iss}	Input Capacitance	—	640	—	pF	V_{GS}=0V, V_{DS}=25V, f=1.0MHz
C_{oss}	Output Capacitance	—	240	—	pF	
C_{rss}	Reverse Transfer Capacitance	—	72	—	pF	
$t_{d(on)}$	Turn-On Delay Time	—	10	15	ns	V_{DD}=0.5BV_{DSS}, I_D=8.3A, Z_O=12Ω (MOSFET switching times are essentially independent of operating temperature)
t_r	Rise Time	—	34	51	ns	
$t_{d(off)}$	Turn-Off Delay Time	—	23	35	ns	
t_f	Fall Time	—	24	36	ns	
Q_g	Total Gate Charge (Gate-Source Plus Gate-Drain)	—	17	26	nC	V_{GS}=10V, I_D=14A, V_{DS}=0.8 Max. Rating (Gate charge is essentially independent of operating temperature.)
Q_{gs}	Gate-Source Charge	—	3.7	5.5	nC	
Q_{gd}	Gate-Drain ("Miller") Charge	—	7	11	nC	

THERMAL RESISTANCE

Symbol	Characteristic		IRF530-3	IRFP130-3	Unit	
R_{thJC}	Junction-to-Case	MAX	1 62	1.62	K/W	
R_{thCS}	Case-to-Sink	TYP	0.5	0.24	K/W	Mounting surface flat, smooth, and greased
R_{thJA}	Junction-to-Ambient	MAX	80	40	K/W	Free Air Operation

Notes: (1) T_J=25°C to 150°C
(2) Pulse test: Pulse width≤300μs, Duty Cycle≤2%
(3) Repetitive rating: Pulse width limited by max. junction temperature

IRF530/531/532/533 IRFP130/131/132/133

N-CHANNEL POWER MOSFETS

SOURCE-DRAIN DIODE RATINGS AND CHARACTERISTICS

Symbol	Characteristic	Min	Typ	Max	Units	Test Conditions
I_S	Continuous Source Current (Body Diode) IRF530/IRFP130 IRF531/IRFP131	—	—	14	A	Modified MOSFET symbol showing the integral reverse P-N junction rectifier 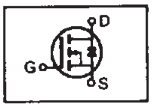
	IRF532/IRFP132 IRF533/IRFP133	—	—	12	A	
I_{SM}	Pulse Source Current(Body Diode)(3) IRF530/IRFP130 IRF531/IRFP131	—	—	56	A	
	IRF532/IRFP132 IRF533/IRFP133	—	—	48	A	
V_{SD}	Diode Forward Voltage (2) IRF530/IRFP130 IRF531/IRFP131	—	—	2 5	V	$T_C=25°C$, $I_S=14A$, $V_{GS}=0V$
	IRF532/IRFP132 IRF533/IRFP133	—	—	2.3	V	$T_C=25°C$, $I_S=12A$, $V_{GS}=0V$
t_{rr}	Reverse Recovery Time	—	120	250	ns	$T_j=25°C$, $I_F=14A$, $dI_F/dt=100A/\mu S$

Notes: (1) $T_J=25°C$ to $150°C$ (2) Pulse test: Pulse width$\leq300\mu s$, Duty Cycle$\leq2\%$
(3) Repetitive rating: Pulse with limited by max junction temperature

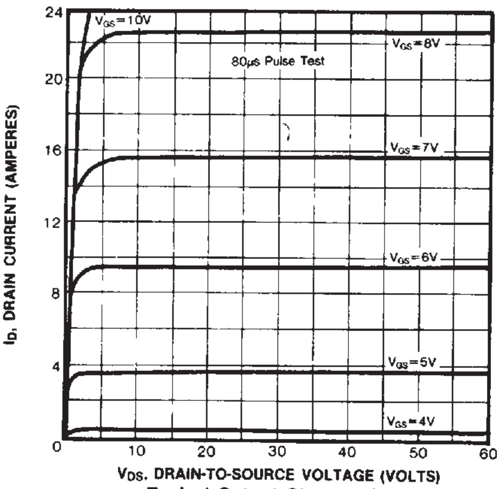

Typical Output Characteristics

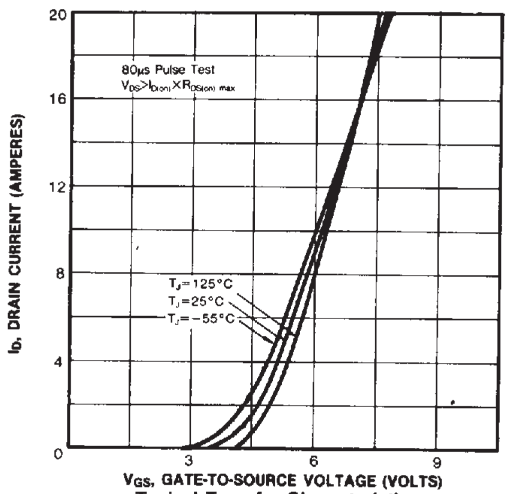

Typical Transfer Characteristics

IRF530/531/532/533
IRFP130/131/132/133

N-CHANNEL POWER MOSFETS

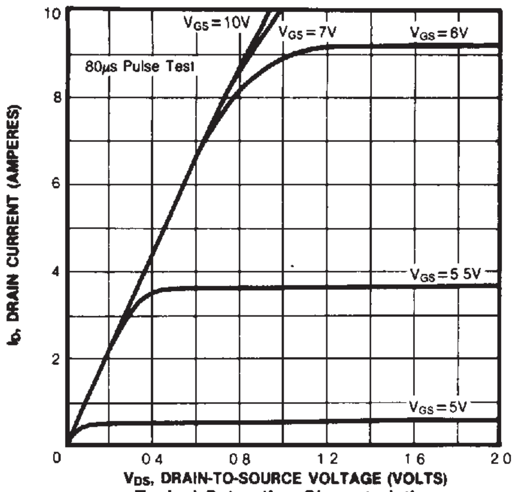

Typical Saturation Characteristics

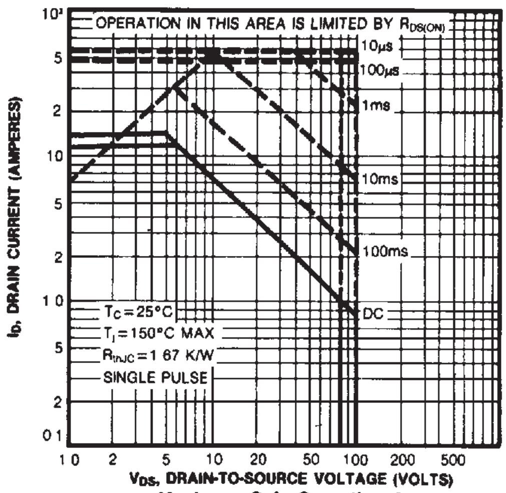

Maximum Safe Operating Area

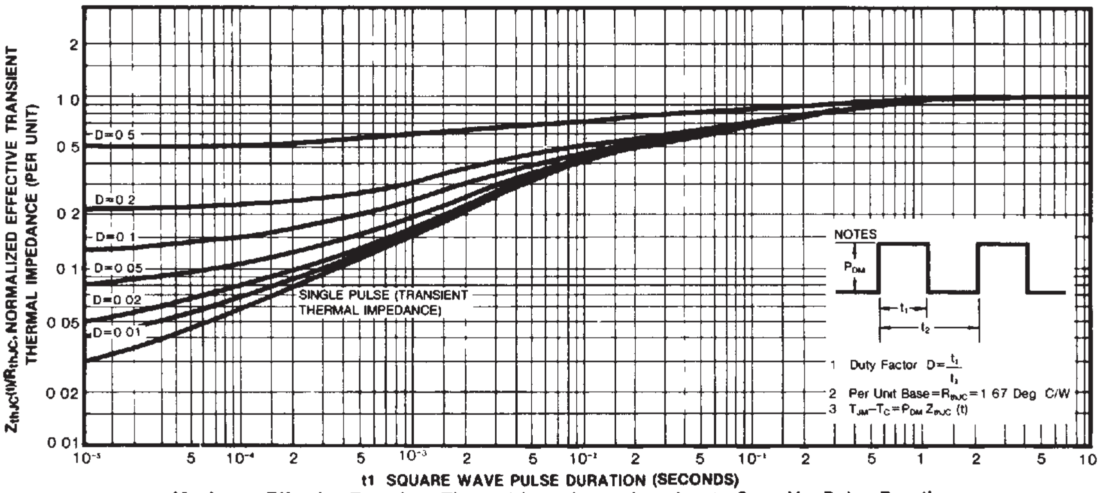

Maximum Effective Transient Thermal Impedance Junction-to-Case Vs. Pulse Duration

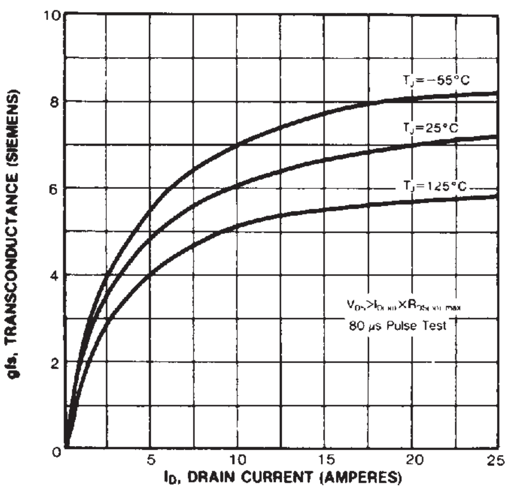

Typical Transcounductance Vs. Drain Current

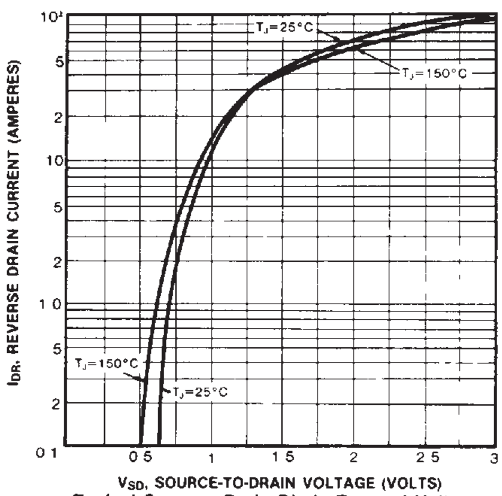

Typical Source—Drain Diode Forward Voltage

2

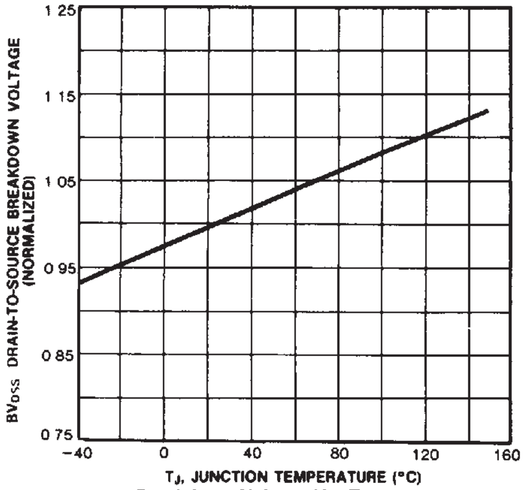

Breakdown Voltage Vs. Temperature

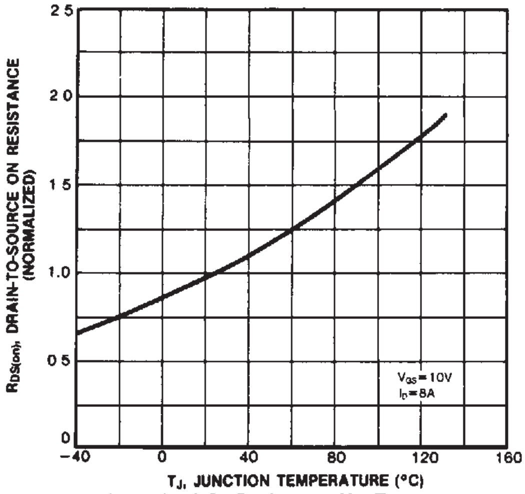

Normalized On-Resistance Vs. Temperature

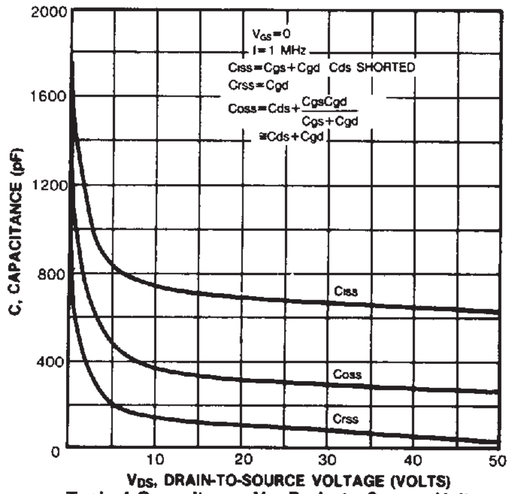

Typical Capacitance Vs. Drain to Source Voltage

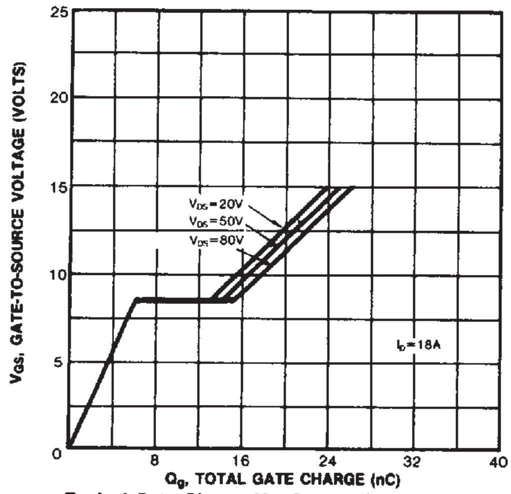

Typical Gate Charge Vs. Gate-To-Source Voltage

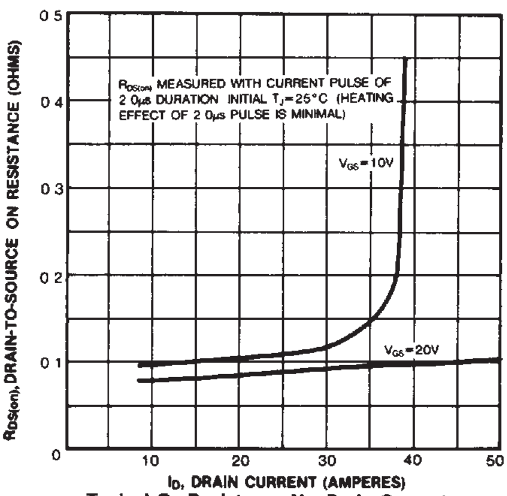

Typical On-Resistance Vs. Drain Current

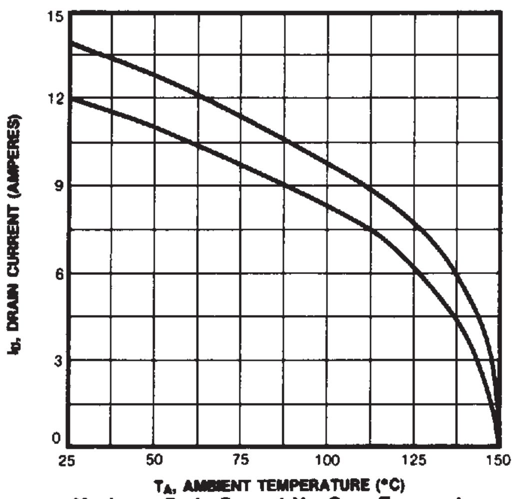

Maximum Drain Current Vs. Case Temperature

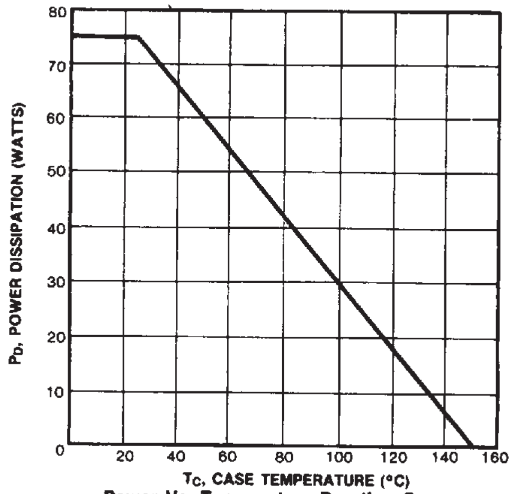

Power Vs. Temperature Derating Curve